© JUL 2026 | IRE Journals | Volume 10 Issue 1 | ISSN: 2456-8880
DOI: https://doi.org/10.64388/IREV10I1-1719581

Mathematical Model for The Dynamics of Nutrient-Phytoplankton System with Delay Under Climate Change and Deoxygination of Oceans

USMAN SOLOMON ALANI[1], IBRAHIM ISA ADAMU[2], SHAMTANG BENSHAK MUSA[3]
[1]*Department of mathematics, Modibbo Adama University Yola, Adamawa state, Nigeria.*
[2] *Department of mathematics, Federal Polytechnic Kaltungo, Gombe state, Nigeria.*
[3]*Department of Statistics, Federal Polytechnic Kaltungo, Gombe state, Nigeria.*

Abstract- ***Marine plankton ecosystems are fundamental to global oxygen production and carbon sequestration, yet they are increasingly threatened by ocean deoxygenation, and climate change. This study proposes a novel six-dimensional delayed differential equation model that captures the complex interactions among nutrient concentration (N), phytoplankton biomass (P), zooplankton biomass (Z), dissolved oxygen (O), upper ocean temperature (T), and greenhouse gas concentration (G). Three discrete time delays account for phytoplankton decomposition, zooplankton decomposition, and toxin maturation in phytoplankton. Existence and uniqueness of solutions are established using the Lipschitz condition. Positivity of solutions and boundedness in a positively invariant region are rigorously proved via comparison theorems, while local asymptotic stability of coexistence and temperature-zero equilibria is proven via linearization and the Routh-Hurwitz criteria. Numerical simulations reveal that baseline parameters induce rapid deoxygenation, with dissolved oxygen falling below 0.5 ppm within 15 days despite an initial phytoplankton bloom. Two scenarios sustain high dissolved oxygenation: (i) fixing temperature at 0 °C, which eliminates warming-induced oxygen loss and thermal inhibition of phytoplankton, and (ii) a minimal-deoxygenation case featuring enhanced photosynthetic production, reduced decomposition demand, and efficient greenhouse gas removal. In contrast, moderate and severe deoxygenation scenarios produce hypoxic conditions or complete plankton collapse. Notably, the selected delays (2.5, 4.0, 5.5 days) do not qualitatively alter long-term dynamics compared to delay-free simulations. These findings provide quantitative thresholds for preventing catastrophic dissolved oxygen depletion and highlight the critical roles of thermal stress and nutrient management in preserving marine ecosystem resilience under climate change.***

Keywords: Anoxic, Climate Change, Deoxygenation, Hypoxic, Plankton.

I. INTRODUCTION

Oxygen Production

The ocean plays a central role in sustaining life on Earth. It constitutes approximately 97% of the planet's habitable space and is responsible for producing about 50%–70% of Earth's oxygen (Laffoley *et al*., 2019; Sekerci and Petrovskii, 2015; NOAA, 2024).

This oxygen production is primarily driven by oceanic plankton (*microscopic organisms that drift in aquatic environments*), including algae and photosynthetic bacteria. Notably, Prochlorococcus, one of the smallest photosynthetic organisms, contributes up to 20% of global oxygen production, exceeding the contribution of all tropical rainforests combined (NOAA, 2024).

Marine Ecosystem

Plankton forms the foundation of marine ecosystems. They include diverse species such as diatoms, dinoflagellates, krill, and copepods (Pachiappan *et al*., 2018). Plankton are broadly divided into phytoplankton and zooplankton.

Phytoplankton are photosynthetic organisms that occupy the first trophic level in aquatic food chains and serve as the primary source of food for many aquatic species, Zooplankton, on the other hand, are animal-like plankton that feed on phytoplankton and serve as a link between primary producers (phytoplankton and other photosynthetic organisms that form the base of the aquatic food web) and higher trophic levels (Rehim *et al*., 2016; Sterpu *et al*., 2023).

As observed above, in addition to supporting food webs, Phytoplankton and function as play a vital role in producing oxygen and absorbing carbon dioxide, thereby contributing to the regulation of global climate (Rehim *et al*., 2016), and function as biological indicators of water quality (Octavina *et al*., 2025; Wang *et al*., 2026).

However, excessive growth of phytoplankton can lead to eutrophication, a condition caused by nutrient enrichment (e.g., nitrogen and phosphorus), which results in excessive biomass production and rapid reproduction. This process depletes dissolved oxygen as decomposing organisms (bacteria) consume oxygen, ultimately leading to the death of aquatic organisms and degradation of water quality (Scavia *et al*., 2024).

Dissolved oxygen is critical for marine life. In well-oxygenated waters, oxygen levels can reach up to 10 ppm. However, when levels fall below 5 ppm, aquatic organisms begin to experience stress. Severe hypoxia occurs at levels below 2 ppm, while extreme conditions known as “dead zones” occur when oxygen levels drop below 0.5 ppm, leading to mass mortality of marine organisms (Dybas, 2005).

Over recent decades, ocean deoxygenation has emerged as a significant environmental concern. Dissolved oxygen levels have declined by approximately 2% since the 1960s, particularly in the upper ocean layers (Schmidtko *et al*., 2017; Kolodziejczyk *et al*., 2024).

Future projections suggest that oxygen levels could decrease by up to 7% by the year 2100 due to warming-induced reductions in oxygen solubility and decreased ocean ventilation caused by stratification (Schmidtko *et al*., 2017). The expansion of anoxic waters poses serious threats to marine ecosystems.

Environmental pollution

Before the Industrial Revolution, atmospheric carbon dioxide levels remained relatively stable at about 280 ± 10 ppm (Venegas *et al*., 2023; Wadanambi *et al*., 2020). However, industrialization led to a significant increase in greenhouse gas emissions due to fossil fuel combustion, deforestation, and industrial activities (Prentice *et al*.., 2001; Houghton *et al*., 1990; Sabine *et al*., 2004; Mikaloff *et al*., 2006; Le Quéré *et al*., 2010; Yoro and Daramola, 2020).

These emissions have disrupted the atmospheric balance and intensified climate change (Martin *et al*., 2017; Hartmann *et al*., 2013). Recent data indicate that atmospheric CO2 levels reached 421.08 ppm in 2023, with further increases recorded in 2024 and 2025 (Statista, 2024; NOAA, 2025). This rise enhances the greenhouse effect, leading to global warming, changes in precipitation patterns, and increased frequency of extreme weather events (Pachauri and Meyer, 2014).

The oceans absorb approximately 90% of the excess heat generated by greenhouse gas emissions, leading to increased ocean temperatures and heat content (Rhein et al., 2013; Johnson et al., 2018; Von Schuckmann *et al*., 2020; Loeb *et al*., 2021; Cheng *et al*., 2024; Gulev *et al*., 2021). These changes contribute to climate phenomena such as El Niñosuch as sea surface temperature anomalies in the Niño3.4 region ((5°N-5°S, 120°-170°W)) (Zhu *et al*., 2016; Li *et al*., 2023; Cheng *et al*., 2024).

In addition to thermal effects, nutrient pollution poses a major threat to marine ecosystems. Nutrients such as nitrogen and phosphorus enter water bodies through agricultural runoff, wastewater discharge, and other human activities (Carpenter *et al*., 1998; Crain *et al*., 2008; Halpern *et al*., 2008; Smith and Schindler, 2009; Devlin and Brodie, 2023).

These nutrients stimulate phytoplankton blooms, which eventually die and decompose, consuming oxygen and creating hypoxic conditions. Dissolved oxygen (DO) depletion, which appears as hypoxia or anoxia, is a major consequence of eutrophication in coastal waters (Akagha *et al*., 2020).

The decomposition of organic matter by bacteria consumes significant amounts of oxygen, exacerbating oxygen depletion (Nixon, 1998). Sampling conducted at three sites around the Lagos-Epe Lagoon: Ikosi, Imope, and Egbin with the most intense blooms occurring at Ikosi (approximately 6.5°N, 3.9°E) (Akagha *et al*., 2020). Hypoxic conditions (DO $\leq$ 2.6 mg/L) occurred at all three sites in January 2013, and at Ikosi (DO $\leq$ 5 mg/L) in

January 2014, due to algal blooms and microbial decomposition of organic matter.

Mathematical Models

A good number of mathematical models has been proposed to understand the interaction among species in the plankton ecosystem and their dynamical properties (Chen *et al.* 2015; Sekerci and Petrovskii 2015; Sekerci and Ozarslan 2020). Others like Mandal *et al.* (2021a), Mandal *et al.* (2021b), and Ochieng (2024) proposed mathematical models to understand the effects of increasing greenhouse gas emissions on climate change.

These dynamical properties mainly include existence and uniqueness of solutions, positivity of solutions, and stability i.e for equilibria, instability, global stability, and Hopf bifurcation (Rehim *et al.* 2016; Thakur *et al.* 2021).

Chen *et al.* (2015) proposed a mathematical model to investigate the dynamics of temperature and light on the growth of phytoplankton in shallow lake ecosystems. In developing their model, they assumed that the lake is a well-mixed and physically homogeneous system with no spatial gradients in nutrient or phytoplankton concentrations.

They further assumed that phytoplankton growth depends on nutrient availability, water temperature, and light intensity, with nutrient inputs originating from external sources and sediment release, while phytoplankton losses occur through natural mortality and intraspecific competition.

The authors also assumed that light penetration decreases with increasing water depth and phytoplankton density according to the Beer–Lambert law and that the combined effects of nutrient, temperature, and light on phytoplankton growth are multiplicative.

They adopted a compartmental modelling approach to formulate a system of two nonlinear differential equations consisting of phytoplankton biomass A(t) and nutrient concentration P(t). The analytical results of their study defined an ecological reproductive index R_0; when $R_0 < 1$, the phytoplankton-free equilibrium is globally stable (phytoplankton cannot persist), whereas when $R_0 > 1$, a unique interior equilibrium exists and is globally stable (phytoplankton survives).

Numerical simulations revealed that R_0 and equilibrium phytoplankton density increase with temperature up to an optimum (about 28°C) and then decrease, increase with light intensity, decrease with mixing depth, and increase with nutrient input.

The results of their study further demonstrated that the model predictions agreed well with experimental data on Microcystis aeruginosa from Xinlicheng Reservoir.

Consequently, the authors concluded that the interaction of temperature, light, and nutrient availability plays a fundamental role in triggering phytoplankton blooms and that controlling nutrient inputs remains one of the most effective strategies for preventing excessive phytoplankton proliferation in shallow lake ecosystems.

Sekerci and Petrovskii (2015) proposed a mathematical model to investigate plankton–oxygen dynamics under climate change. In developing their model, they assumed that phytoplankton produce oxygen through photosynthesis and consume oxygen through respiration, while zooplankton feed on phytoplankton and consume oxygen through breathing.

They further assumed that oxygen production is influenced by environmental conditions, particularly water temperature, that phytoplankton growth depends on oxygen availability and is regulated by intraspecific competition, and that zooplankton feeding follows a Holling type II functional response with feeding efficiency dependent on oxygen concentration.

The authors also assumed that oxygen is naturally depleted through biochemical processes in the aquatic environment and that climate-induced warming alters the rate of oxygen production by phytoplankton. They adopted a compartmental modelling approach to formulate a system of three

nonlinear differential equations consisting of oxygen concentration c(t), phytoplankton density u(t), and zooplankton density v(t).

The analytical results of their study established the existence and stability properties of extinction, boundary, and coexistence equilibrium states and revealed the occurrence of bi-stability, tri-stability, Hopf bifurcation, and limit-cycle oscillations under different parameter regimes. Numerical simulations showed that sustainable oxygen production is possible only within an intermediate range of oxygen production rates, while excessively low or high production rates destabilize the ecosystem.

The results further demonstrated that climate-driven changes in oxygen production can trigger increasing oscillations in oxygen and plankton populations, ultimately leading to oxygen depletion and plankton extinction. Consequently, the authors concluded that global warming has the potential to induce catastrophic ecological collapse in marine ecosystems by disrupting oxygen production and threatening the persistence of plankton communities that sustain oceanic life and contribute significantly to atmospheric oxygen production.

Rehim *et al.* (2016) proposed a mathematical model to investigate the dynamics of a nutrient–plankton ecosystem in the presence of toxin-producing phytoplankton and time-delay effects. In developing their model, they assumed that nutrient serves as the primary resource for phytoplankton growth, while zooplankton depend exclusively on phytoplankton as their food source and do not consume nutrients directly.

They further assumed that nutrient uptake by phytoplankton follows a Holling type I functional response, whereas zooplankton grazing and toxin-induced mortality follow Holling type II functional responses. The authors also assumed that the release of toxins by phytoplankton is not instantaneous but occurs after a maturation period and that nutrient recycling from dead phytoplankton and zooplankton populations is mediated through decomposition delays.

In addition, phytoplankton were assumed to experience intraspecific competition due to limited environmental resources. They adopted a compartment modeling approach to formulate a system of three delay differential equations: dissolved nutrient concentration N(t), phytoplankton density p(t), and zooplankton density z(t).

The analytical results of their study established the existence of three equilibria (extinction, zooplankton-eradication, and coexistence), derived conditions for local and global asymptotic stability, and proved that time delays can destabilize the coexistence equilibrium via Hopf bifurcation, leading to periodic oscillations.

Numerical simulations revealed that when the delay is below a critical threshold ($\tau_0 = 1.7657$), the coexistence equilibrium remains stable, but exceeding this threshold induces stable limit cycles.

The results of their study further demonstrated that with unequal delays ($\tau_1 \neq \tau_2 \neq \tau_3$), stability switches occur multiple times as delays increase, with the system alternating between stable and unstable behavior. Consequently, the authors concluded that time lags in nutrient recycling and toxin production play a crucial role in phytoplankton bloom dynamics, and that ignoring such delays may lead to incorrect predictions of ecosystem stability and the onset of harmful algal blooms. They recommended an average conversion rate.

Thakur *et al.* (2021) proposed a mathematical model to investigate delay-induced stability transitions in nutrient–plankton systems in the presence of toxic phytoplankton. In developing their model, they assumed that nutrient uptake by phytoplankton follows Holling type II functional response, while zooplankton grazing and toxin-induced extra mortality of zooplankton both follow Monod-Haldane (Holling type IV) functional response. Nutrient recycling from dead phytoplankton is included without time delay, and phytoplankton exhibit intra-specific competition.

Toxin liberation by phytoplankton is not instantaneous but requires a discrete time delay for phytoplankton maturity.

They adopted a compartment modeling approach to formulate a system of three equations: nutrient concentration N(t), phytoplankton density P(t), and zooplankton density Z(t). The analytical results of their study established uniform boundedness, existence of feasible equilibria, local stability conditions for the delay-free system, and derived the critical delay (τ^* = 4.2156) at which Hopf bifurcation occurs, along with the direction and stability of bifurcating periodic solutions. Numerical simulations revealed that below the critical delay the system is stable, while beyond (τ^*) limit cycles appear; further increase in delay leads to stability switches and eventually chaotic dynamics (at τ = 24 days).

The results of their study further demonstrated that higher toxin production rate ρ drives zooplankton to extinction, whereas lower ρ stabilizes the system; increasing nutrient input N_0 induces high-amplitude fluctuations, while decreasing it stabilizes chaos; and higher absorption rate a or higher intra-specific competition γ also stabilize the dynamics.

Consequently, the authors concluded that time delay in toxin liberation is a key factor triggering planktonic blooms and chaos, but these adverse effects can be mitigated by controlling nutrient input, toxin production, and phytoplankton competition rates.

Mandal *et al.* (2021a), proposed a mathematical model to understand the effect of atmospheric temperature on the planktonic ecosystem in oceans. In developing their model, they assumed that phytoplankton photosynthesis is temperature-dependent, with optimal activity near 25°C, and that phytoplankton growth is influenced by both temperature and dissolved oxygen concentration.

Zooplankton are assumed to feed exclusively on phytoplankton, while dissolved oxygen is produced through photosynthetic activity and consumed by zooplankton respiration, phytoplankton respiration, and natural depletion. They adopted a compartment modeling approach to formulate a system of four nonlinear ordinary differential equations representing atmospheric temperature T(t), phytoplankton density P(t), zooplankton density Z(t), and dissolved oxygen concentration D(t).

The analytical results of their study established the positivity and boundedness of the system, along with stability conditions at three equilibrium points. Numerical simulations revealed that at the optimum temperature (25°C), photosynthetic activity and growth rates of phytoplankton, zooplankton, and dissolved oxygen reach their maximum, resulting in a stable and balanced marine ecosystem.

In contrast, at lower (18°C) or higher (30°C) temperatures, photosynthetic efficiency declines, leading to reduced growth of phytoplankton and zooplankton and lower oxygen production. The results of their study further demonstrated that deviations from the optimal temperature destabilize the plankton-oxygen dynamics. Consequently, the authors concluded that maintaining stable atmospheric temperatures is critical for sustaining the marine planktonic food web and that rising temperatures due to climate change could severely disrupt ocean ecosystem health.

Mandal *et al.* (2021b), proposed a mathematical model to understand the potential impact of climate change on living beings near coastal areas. In developing their model, they assumed that GHGs increase through natural processes, human activities, and natural disasters, while forests absorb a portion of these gases.

Atmospheric temperature rises due to increasing GHG concentrations and human activities but is moderated by forest ecosystems. Human populations are assumed to grow logistically while being adversely affected by elevated temperatures and GHG emissions, whereas forest ecosystems also grow logistically but are degraded by human activities and climate-induced stress.

They adopted compartment modeling approach to usher in a system of four equations: greenhouse gases G(t), atmospheric temperature C(t), human population H(t), and forest ecosystem E(t). The analytical results of their study established the positivity, boundedness, and stability of the system,

while the numerical simulations revealed that increasing GHG emissions lead to significant rises in atmospheric temperature, accelerated climate change, declining forest coverage, and reduced human population growth.

The results of their study further demonstrated that deforestation weakens the environment's ability to absorb GHGs, creating a feedback mechanism that intensifies global warming and ecosystem degradation. Consequently, the authors concluded that continued greenhouse gas emissions and deforestation could severely destabilize environmental systems and threaten the sustainability of life in coastal regions if effective mitigation measures are not implemented.

Ochieng (2024), proposed a novel data-driven dynamical model to predict future climate trends in Nairobi, Kenya, focusing on CO_2 emissions, photosynthetic biomass, human population, and atmospheric temperature. In developing his model, he assumed that excessive CO_2 accumulation is solely responsible for climate change, that both photosynthetic biomass and human population grow logistically.

Atmospheric temperature rises due to CO_2-driven greenhouse effects and human activities, while photosynthetic biomass absorbs CO_2 and mitigates warming, but is reduced by human-induced deforestation and climate-related stress. They adopted a compartmental modeling approach to formulate a system of four equations: carbon dioxide concentration C(t), photosynthetic biomass density B(t), human population density N(t), and atmospheric temperature T(t).

The analytical results of their study derived a concentration number ($C^* = 2027.43 > 1$), indicating a high risk of excessive long-term CO_2 accumulation, and sensitivity analysis identified the intrinsic CO_2 accumulation rate and human birth/immigration rate as the most influential parameters.

Numerical simulations, calibrated with historical Nairobi climate data (January 2022 – February 2024) using least-squares curve fitting, achieved a mean absolute error of 0.0884 for temperature, confirming good model fit.

The results of their study further projected that from May 2024, CO_2 concentration may fall below 400 ppm, photosynthetic biomass density may decline to 5–20 kg/m², human population density may rise sharply from 0.5 to 2.8 people/km² then drop, and atmospheric temperature may increase from 17.5°C (September 2024) to 32°C (January 2025) before a sharp decrease.

Consequently, the author concluded that these findings underscore the urgency of implementing targeted mitigation and adaptation strategies to address potential climate-driven population movements, resource scarcity, and positive feedback loops in Nairobi's climate system.

Sarkar *et al.* (2025) proposed a mathematical model to investigate the influence of global warming on carbon, phytoplankton, and zooplankton dynamics in marine ecosystems. In developing their model, they assumed that atmospheric carbon dioxide continuously mixes with ocean water at a constant rate, while phytoplankton consume carbon during photosynthesis and release it through respiration.

Zooplankton were assumed to feed on phytoplankton and contribute to carbon production through metabolic respiration. The authors further assumed that sufficient oxygen is available in the marine environment for respiration, that carbon consumption by phytoplankton exceeds carbon production through respiration, and that phytoplankton growth follows a logistic growth pattern.

They adopted a compartmental modelling approach to formulate a system of three nonlinear differential equations consisting of carbon concentration C(t), phytoplankton biomass P(t), and zooplankton biomass Z(t).

The analytical results of their study established positivity, boundedness, existence of three equilibria (phytoplankton-zooplankton-free, zooplankton-free, and coexisting), and local stability conditions using the Routh-Hurwitz criterion, while the numerical simulations revealed that the carbon capturing

© JUL 2026 | IRE Journals | Volume 10 Issue 1 | ISSN: 2456-8880
DOI: https://doi.org/10.64388/IREV10I1-1719581

coefficient α_1 induces Hopf bifurcation: for low α_1 the system is stable, for intermediate α_1 limit cycles appear, and for high α_1 stability returns. The results of their study further demonstrated that increasing the carbon capturing coefficient reduces carbon concentration while increasing zooplankton density, and that spatial diffusion leads to Turing instability and patchy pattern formation.

When global warming was introduced as a time-varying carbon emission rate, the model predicted shifts in plankton seasonal dynamics (phase differences and amplitude increases) consistent with experimental observations.

Consequently, the authors concluded that increasing carbon capture by phytoplankton can lower ocean carbon levels, but global warming alters plankton seasonal dynamics, and future research should incorporate environmental factors such as pH, temperature, and light to better predict ecosystem responses.

Despite extensive research on nutrient-plankton, and climate related systems, the comparative study of nutrient-plankton interaction with delay, ocean deoxygenation, and the effects of greenhouse gas emissions on climate change, within the aquatic ecosystems is still absent.

With this motivation, we set out to develop a mathematical model on nutrient-plankton system with delay under ocean deoxygenation and climate change.

II. MODEL FORMULATION

The model is formulated based on the following assumptions:

i. It is assumed that that the system is a well-mixed system.
ii. Phytoplankton growth is limited by nutrients availability.
iii. The consumption of oxygen by microbes as they breakdown dead phytoplankton is higher than the production of oxygen by the phytoplankton.
iv. Zooplankton grazes on phytoplankton, while fish and other aquatic animals predate on zooplankton.
v. Temperature dynamics are affected by anthropogenic climate change.
vi. The release of toxic substances by phytoplankton species is not an immediate process; instead, it is influenced by a time delay necessary for the species to reach maturity.

III. THE MODEL

Table 1: Variables

Variable	Descriptions
$N(t)$	Nutrient concentration at time t.
$P(t)$	Phytoplankton biomass at time t.
$Z(t)$	Zooplankton biomass at time t.
$O(t)$	Dissolved Oxygen concentration at time t.
$T(t)$	Temperature of the upper ocean at time t.
$G(t)$	Greenhouse gas concentration at time t.

Table 2: Parameters

Parameter	Description
D	Washout rate.
w	Microbial decomposition efficiency factor.
N_0	Constant input of nutrient concentration.
a	Half-saturation constant.
x	Temperature decrease rate due to heat loss to the atmosphere and ocean circulation.
v	Self-shading rate
k_1	The conversion factor from nutrient to phytoplankton (where $0 < k_1 < 1$).
k_2	The conversion factor from phytoplankton to zooplankton (where $0 < k_2 < 1$).
k_3	The rate of toxic substances produced by per unit biomass of phytoplankton.
f	Rate of greenhouse gas increase due to

© JUL 2026 | IRE Journals | Volume 10 Issue 1 | ISSN: 2456-8880
DOI: https://doi.org/10.64388/IREV10I1-1719581

	increase in nutrient availability.
m_1	Rate nutrient production due to mortality of phytoplankton population$0 < m_1 < 1$.
m_2	Rate nutrient production due to mortality of zooplankton population where $0 < m_2 < 1$.
d_1	Natural mortality rate of phytoplankton.
d_2	Natural mortality rate of zooplankton.
h	Rate of inhibition of phytoplankton population growth by temperature.
ε	Rate of temperature production due to the interaction between zooplankton and temperature.
α	Nutrient uptake rate by the phytoplankton.
ϕ	Greenhouse production rate due to respiration of the zooplankton.
β	The maximum rate of zooplankton ingestion of phytoplankton.
δ	Rate of oxygen consumption due to waste decomposition.
ψ	Rate of oxygen production due to

	photosynthesis.
μ	Rate of oxygen depletion due to increased temperature.
π_1	Rate of oxygen consumption due to phytoplankton respiration.
π_2	Oxygen consumption by zooplankton respiration
π_3	Rate of oxygen consumption due to zooplankton respiration.
σ	Rate of nutrient depletion due to temperature effects on nutrient cycling.
θ_1	Rate of temperature increase due to increase in greenhouse gases.
θ_2	Rate of greenhouse gas removal through ocean circulation, sedimentation, and atmospheric exchange.
τ_1	Time delay linked with the decomposition of the phytoplankton population.
τ_2	Time delay parameter for the decomposition of the zooplankton population.
τ_3	Time delay period required for the maturity of toxic-phytoplankton.

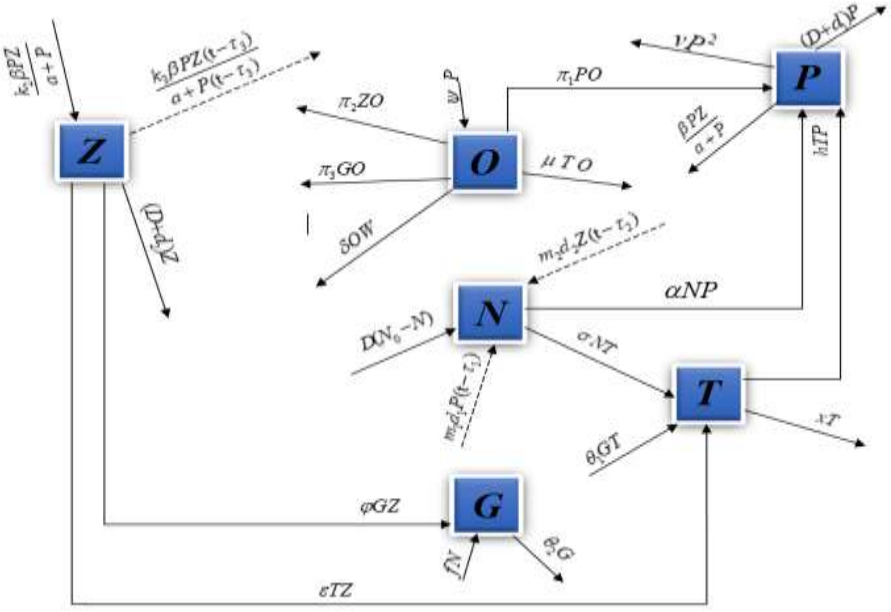

Figure 1: Flow diagram of the model

© JUL 2026 | IRE Journals | Volume 10 Issue 1 | ISSN: 2456-8880
DOI: https://doi.org/10.64388/IREV10I1-1719581

IV. THE MODEL EQUATION

$$\frac{dN}{dt} = D(N_0 - N) - \alpha NP + m_1 d_1 P(t-\tau_1) + m_2 d_2 Z(t-\tau_2) - \sigma NT \quad (3.0)$$

$$\frac{dZ}{dt} = \frac{k_2 \beta PZ}{a+P} - \frac{k_3 \beta ZP(t-\tau_3)}{a+P(t-\tau_3)} - (D+d_2)Z - \varepsilon TZ - \phi GZ \quad (3.1)$$

$$\frac{dO}{dt} = \psi P - \mu TO - \delta wO - \pi_1 PO - \pi_2 ZO - \pi_3 GO \quad (3.2)$$

$$\frac{dP}{dt} = k_1 \alpha NP - (D+d_1)P - \frac{\beta PZ}{a+P} - vP^2 - hTP + \pi_1 PO \quad (3.3)$$

$$\frac{dT}{dt} = \theta_1 GT + \sigma NT - xT + \varepsilon TZ \quad (3.4)$$

$$\frac{dG}{dt} = fN - \theta_2 G + \phi GZ \quad (3.5)$$

With initial condition

$$N(0)=N_0>0, Z(0)=Z_0>0, O(0)=O_0>0, P(0)=P_0>0, T(0)=T_0\geq 0, G(0)=G_0>0$$

V. EXISTENCE AND UNIQUENESS OF SOLUTION OF THE MODEL

We state the theorem and lemma and use it to proof the existence and uniqueness of the solution of the system of equation (3.0) - (3.5). Firstly, we state the Lipchitz condition in the form of a lemma as follows:
Lipchitz condition

Lemma 1: if $g(t,N,Z,O,P,T,G)$ and its partial derivatives $\frac{\partial g_i}{\partial N}, \frac{\partial g_i}{\partial Z}, \frac{\partial g_i}{\partial O}, \frac{\partial g_i}{\partial P}, \frac{\partial g_i}{\partial T}, \frac{\partial g_i}{\partial G}$ are continuous,

and that;

$$\left\| g(t,N_1,Z_1,O_1,P_1,T_1,G_1) - g(t,N_2,Z_2,O_2,P_2,T_2,G_2) \right\| \leq k \left\| (N_1,Z_1,O_1,P_1,T_1,G_1) - (N_2,Z_2,O_2,P_2,T_2,G_2) \right\|$$

, on a bounded convex domain

$$D = \left\{ \left(t, (N,Z,O,P,T,G)\right) \middle| \, |t-t_0| \leq a \right.$$

,

$$\left. \left\| (N,Z,O,P,T,G) - (N_0,Z_0,O_0,P_0,T_0,G_0) \right\| \leq b \right\}$$

then $g(t,N,Z,O,P,T,G)$ satisfies a Lipchitz condition in D, where k is called the Lipchitz constant.

Existence and uniqueness theorem
Theorem 1: Let D denote the region

$$D = \left\{ \left(t, (N,Z,O,P,T,G)\right) \middle| \, |t-t_0| \leq a \right.$$

,

$$\left. \left\| (N,Z,O,P,T,G) - (N_0,Z_0,O_0,P_0,T_0,G_0) \right\| \leq b \right\}$$

,

and suppose that $g(t,N,Z,O,P,T,G)$ satisfied the Lipchitz condition, then, there exist a constant $\delta > 0$ such that there exist a unique continuous vector solution $(N(t),Z(t),O(t),P(t),T(t),G(t))$ to the model equations in the interval $|t-t_0| \leq \delta$.

Proof of Existence and Uniqueness

Let

$$\begin{cases} g_1 = D(N_0 - N) - \alpha NP + m_1 d_1 P(t-\tau_1) + m_2 d_2 Z(t-\tau_2) - \sigma NT \\ g_2 = \frac{k_2 \beta PZ}{a+P} - \frac{k_3 \beta ZP(t-\tau_3)}{a+P(t-\tau_3)} - (D+d_2)Z - \varepsilon TZ - \phi GZ \\ g_3 = \psi P - \mu TO - \delta wO - \pi_1 PO - \pi_2 ZO - \pi_3 GO \\ g_4 = k_1 \alpha NP - (D+d_1)P - \frac{\beta PZ}{a+P} - vP^2 - hTP + \pi_1 PO \\ g_5 = \theta_1 GT + \sigma NT - xT + \varepsilon TZ \\ g_6 = fN - \theta_2 G + \phi GZ \end{cases} \quad (3.6)$$

Clearly, all the functions are continuous. Now we move on to show that partial derivatives $\frac{\partial g_i}{\partial N}, \frac{\partial g_i}{\partial Z}, \frac{\partial g_i}{\partial O}, \frac{\partial g_i}{\partial P}, \frac{\partial g_i}{\partial T}, \frac{\partial g_i}{\partial G}$ are continuous for i=1, 2,3,4,5,6.

© JUL 2026 | IRE Journals | Volume 10 Issue 1 | ISSN: 2456-8880
DOI: https://doi.org/10.64388/IREV10I1-1719581

We have for g_1

$$\left|\frac{\partial g_1}{\partial N}\right| = \left|-(D+\alpha P+\sigma T)\right| = D+\alpha P+\sigma T < \infty$$

$$\left|\frac{\partial g_1}{\partial P}\right| = \left|-\alpha N\right| = \alpha N < \infty$$

$$\left|\frac{\partial g_1}{\partial O}\right| = 0 < \infty$$

$$\left|\frac{\partial g_1}{\partial Z}\right| = 0 < \infty$$

$$\left|\frac{\partial g_1}{\partial T}\right| = \left|-\sigma N\right| = \sigma N < \infty$$

$$\left|\frac{\partial g_1}{\partial G}\right| = 0 < \infty$$

and for g_2;

$$\left|\frac{\partial g_2}{\partial N}\right| = 0 < \infty$$

$$\left|\frac{\partial g_2}{\partial P}\right| = \frac{k_2\beta Za}{(a+P)^2} < \infty$$

$$\left|\frac{\partial g_2}{\partial O}\right| = 0 < \infty$$

$$\left|\frac{\partial g_2}{\partial Z}\right| = \left|-\left(\frac{k_3\beta P(\mathrm{t}-\tau_3)}{a+P(\mathrm{t}-\tau_3)} - \frac{k_2\beta P}{a+P} + (D+d_2) + \varepsilon T + \phi G\right)\right|$$

$$= \frac{k_3\beta P(\mathrm{t}-\tau_3)}{a+P(\mathrm{t}-\tau_3)} - \frac{k_2\beta P}{a+P} + (D+d_2) + \varepsilon T + \phi G < \infty$$

$$\left|\frac{\partial g_2}{\partial T}\right| = \left|-\varepsilon Z\right| = \varepsilon Z < \infty$$

$$\left|\frac{\partial g_2}{\partial G}\right| = \left|-\phi Z\right| = \phi Z < \infty$$

for g_3;

$$\left|\frac{\partial g_3}{\partial N}\right| = 0 < \infty$$

$$\left|\frac{\partial g_3}{\partial P}\right| = \psi - \pi_1 O < \infty$$

$$\left|\frac{\partial g_3}{\partial O}\right| = -\left(\delta w + \mu T + \pi_1 P + \pi_2 Z + \pi_3 G\right)$$

$$= \delta w + \mu T + \pi_1 P + \pi_2 Z + \pi_3 G < \infty$$

$$\left|\frac{\partial g_3}{\partial Z}\right| = \left|-\pi_2 O\right| = \pi_2 O < \infty$$

$$\left|\frac{\partial g_3}{\partial T}\right| = \left|-\mu O\right| = \mu O < \infty$$

$$\left|\frac{\partial g_3}{\partial G}\right| = \left|-\pi_3 O\right| = \pi_3 O < \infty$$

for g_4;

$$\left|\frac{\partial g_4}{\partial N}\right| = k_1\alpha P < \infty$$

$$\left|\frac{\partial g_4}{\partial P}\right| = \left|-\left((D+d_1) - k_1\alpha N + \frac{\beta Za}{(a+P)^2} + 2\nu P + hT - \pi_1 O\right)\right|$$

$$= (D+d_1) - k_1\alpha N + \frac{\beta Za}{(a+P)^2} + 2\nu P + hT - \pi_1 O < \infty$$

$$\left|\frac{\partial g_4}{\partial O}\right| = \pi_1 P < \infty$$

$$\left|\frac{\partial g_4}{\partial Z}\right| = \left|-\frac{\beta P}{a+P}\right| = \frac{\beta P}{a+P} < \infty$$

$$\left|\frac{\partial g_4}{\partial T}\right| = \left|-hP\right| = hP < \infty$$

$$\left|\frac{\partial g_4}{\partial G}\right| = 0 < \infty$$

© JUL 2026 | IRE Journals | Volume 10 Issue 1 | ISSN: 2456-8880
DOI: https://doi.org/10.64388/IREV10I1-1719581

$$\left|\frac{\partial g_5}{\partial N}\right| = \sigma T < \infty$$

$$\left|\frac{\partial g_5}{\partial P}\right| = 0 < \infty$$

$$\left|\frac{\partial g_5}{\partial O}\right| = 0 < \infty$$

$$\left|\frac{\partial g_5}{\partial Z}\right| = \varepsilon T < \infty$$

$$\left|\frac{\partial g_5}{\partial T}\right| = \theta_1 G + \sigma N - x + \varepsilon Z < \infty$$

$$\left|\frac{\partial g_5}{\partial G}\right| = \theta_1 T < \infty$$

Finally, for g_6;

$$\left|\frac{\partial g_6}{\partial N}\right| = f < \infty$$

$$\left|\frac{\partial g_6}{\partial P}\right| = 0 < \infty$$

$$\left|\frac{\partial g_6}{\partial O}\right| = 0 < \infty$$

$$\left|\frac{\partial g_6}{\partial Z}\right| = \phi G < \infty$$

$$\left|\frac{\partial g_6}{\partial T}\right| = 0 < \infty$$

$$\left|\frac{\partial g_6}{\partial G}\right| = -\theta_2 + \phi Z < \infty$$

Clearly all the partial derivatives are continuous. Since all the functions $g_i = x_i$ of the model equations and their partial derivatives are continuous in the bounded domain D, by the existence and uniqueness theorem, there exists a unique solution to the model equations (3.0) - (3.5) in the region D.

VI. POSITIVITY AND BOUNDEDNESS OF THE MODEL SOLUTION

We prove that the solution of the model equations from (3.0) - (3.5) are non-negative, remain positive for all time $t \geq 0$, and bounded in a region Ω for all time $t \geq 0$.

Lemma 2:

Let the initial values of the state variables be

$\{N(0) = N_0 > 0,\ Z(0) = Z_0 > 0,$
$O(0) = O_0 > 0,\ P(0) = P_0 > 0,\ T(0) = T_0 \geq 0,$
$G(0) = G_0 > 0\} \in R_+^6$. Then, the solution set $\{N(t), Z(t), O(t), P(t), T(t), G(t)\}$ of the system (3.0) - (3.5) is non-negative for all t > 0.

Proof:

for equation (3.0);

$$\frac{dN}{dt} = D(N_0 - N) - \alpha NP + m_1 d_1 P(t - \tau_1) + m_2 d_2 P(t - \tau_2) - \sigma NT$$

It follows by comparison theorem that

$$\frac{dN}{dt} \geq -(\alpha NP + \sigma NT) \qquad (3.7)$$

Solving (3.7) with the aid of separation of variables, we have

$$\int \frac{dN}{dt} \geq -\int (\alpha NP + \sigma NT)\, dt$$

$$N(t) \geq N(0) e^{-\int (\alpha NP + \sigma NT) dt}$$

$$N(t) \geq N(0) e^{-(\alpha NP + \sigma NT)t} > 0$$

Similarly, for equation 3.1 to 3.5, it can be shown that; Z, O, P, T are all positive

Hence Lemma 2 is proved.

Lemma 3: The closed set

$$\Omega = \left\{ (N, Z, O, P, T, G) \in R_+^6 : N + Z + O + P + T + G = X > 0, 0 \leq X \leq \frac{DN_0}{\lambda} \right\}$$

is positively invariant.

© JUL 2026 | IRE Journals | Volume 10 Issue 1 | ISSN: 2456-8880
DOI: https://doi.org/10.64388/IREV10I1-1719581

Proof:

From the model equations (3.0) - (3.5), the total population is given by

$$X = N + Z + O + P + T + G \tag{3.8}$$

Now;

$$\frac{dX}{dt} = \frac{dN}{dt} + \frac{dZ}{dt} + \frac{dO}{dt} + \frac{dP}{dt} + \frac{dT}{dt} + \frac{dG}{dt} \tag{3.9}$$

Substituting the derivatives of the state variables, we have;

$$\frac{dX}{dt} = DN_0 + (f - D)N + (m_2 d_2 - D - d_2)Z + \left(-\frac{\delta w}{k_1}\right)O + \left(\frac{\psi - D - d_1}{k_1} + m_1 d_1\right)P + (-x)T$$
$$+(-\theta_2)G - \left(\frac{v}{k_1}P^2 + \frac{\mu}{k_1}TO + \frac{\pi_2}{k_1}ZO + \frac{\pi_3}{k_1}GO + \frac{h}{k_1}TP - \left[(k_2 - k_3) - \frac{1}{k_1}\right]\frac{\beta PZ}{a+P} - \theta_1 GT\right) \tag{4.0}$$

Where

$$Z(t-\tau_2) \le Z(t), P(t-\tau_1) \le P(t), P(t-\tau_3) \le P(t)$$

$$\Rightarrow \frac{dX}{dt} = DN_0 - (D - f)N - (D + d_2 - m_2 d_2)Z + \frac{\delta w}{k_1}O - \left(\frac{D + d_1 - \psi}{k_1} - m_1 d_1\right)P + xT$$
$$+\theta_2 G + \left(\frac{v}{k_1}P^2 + \frac{\mu}{k_1}TO + \frac{\pi_2}{k_1}ZO + \frac{\pi_3}{k_1}GO + \frac{h}{k_1}TP - \left[(k_2 - k_3) - \frac{1}{k_1}\right]\frac{\beta PZ}{a+P} - \theta_1 GT\right)$$

Let;

$$DN_0 - (D - f)N - (D + d_2 - m_2 d_2)Z + \frac{\delta w}{k_1}O - \left(\frac{D + d_1 - \psi}{k_1} - m_1 d_1\right)P + xT$$
$$+\theta_2 G = DN_0 - \lambda X$$

and

$$\frac{v}{k_1}P^2 + \frac{\mu}{k_1}TO + \frac{\pi_2}{k_1}ZO + \frac{\pi_3}{k_1}GO + \frac{h}{k_1}TP - \left[(k_2 - k_3) - \frac{1}{k_1}\right]\frac{\beta PZ}{a+P} - \theta_1 GT = \eta$$

But $k_1 \le 1$.

This imply that (4.0) is equivalent to

$$\frac{dX}{dt} = DN_0 - \lambda X + \eta \tag{4.1}$$

Let $\eta \le 0$, so that

$$\frac{dX}{dt} \le DN_0 - \lambda X \tag{4.2}$$

Thus, $\frac{dX}{dt} + \lambda X \le DN_0$ (4.3)

The I.F is $e^{\int \lambda dt} = e^{\lambda t}$

Multiplying both sides of (4.3) by $e^{\lambda t}$ gives

$$e^{\lambda t}\frac{dX}{dt} + \lambda e^{\lambda t} X \le DN_0 e^{\lambda t}$$

$$\frac{d}{dt}\left[Xe^{\lambda t}\right] \le DN_0 e^{\lambda t} \Rightarrow d\left[Xe^{\lambda t}\right] \le DN_0 e^{\lambda t} dt \Rightarrow \int d\left[Xe^{\lambda t}\right] \le DN_0 \int e^{\lambda t} dt + C \Rightarrow X(t) \le \frac{DN_0}{\lambda} + Ce^{-\lambda t}$$

$$\lim_{t\to\infty} X(t) \le \lim_{t\to\infty} \frac{DN_0}{\lambda} + C\lim_{t\to\infty} e^{-\lambda t}$$

$$\lim_{t\to\infty} X(t) \le \lim_{t\to\infty} \frac{DN_0}{\lambda} + C(0)$$

$$\lim_{t\to\infty} X(t) \le \frac{DN_0}{\lambda} \tag{4.4}$$

Thus,

$$\Omega = \left\{(N, Z, O, P, T, G) \in R_+^6 : N + Z + O + P + T + G = X > 0, 0 \le X \le \frac{DN_0}{\lambda}\right\}$$

. Hence Lemma 3 is proved.

VII. THE EQUILIBRIUM POINTS OF THE MODEL

© JUL 2026 | IRE Journals | Volume 10 Issue 1 | ISSN: 2456-8880
DOI: https://doi.org/10.64388/IREV10I1-1719581

The equilibrium points are found by setting the derivatives to zero in the governing equations (3.0) - (3.5). At equilibrium, we assume steady-state conditions for the model equations

$$\frac{dN}{dt}=\frac{dZ}{dt}=\frac{dO}{dt}=\frac{dP}{dt}=\frac{dT}{dt}=\frac{dG}{dt}=0 \tag{4.5}$$

Thus, at equilibrium point, the system of equation becomes;

$$D(N_0-N)-\alpha NP+m_1d_1P(t-\tau_1)+m_2d_2Z(t-\tau_2)-\sigma NT=0 \tag{4.6}$$

$$\frac{k_2\beta PZ}{a+P}-\frac{k_3\beta ZP(t-\tau_3)}{a+P(t-\tau_3)}-(D+d_2)Z-\varepsilon TZ-\phi GZ=0 \tag{4.7}$$

$$\psi P-\mu TO-\delta wO-\pi_1PO-\pi_2ZO-\pi_3GO=0 \tag{4.8}$$

$$k_1\alpha NP-(D+d_1)P-\frac{\beta PZ}{a+P}-vP^2-hTP+\pi_1PO=0 \tag{4.9}$$

$$\theta_1GT+\sigma NT-xT+\varepsilon TZ=0 \tag{5.0}$$

$$fN-\theta_2G+\phi GZ=0 \tag{5.1}$$

7.1 The Equilibrium Points

At the coexistence equilibrium point of our dynamic system, all variables (*N, Z, O, P, T, G*) are potentially nonzero. We set the derivatives to zero and solve the system:

Solving the equations from (5.1), we have;

$$fN-G(\theta_2-\phi Z)=0$$
$$fN=G(\theta_2-\phi Z)$$
$$\Rightarrow G^*=\frac{fN}{\theta_2-\phi Z} \tag{5.2}$$

from (4.6), we have;

$$N(D+\alpha P+\sigma T)=DN_0+m_1d_1P(t-\tau_1)+m_2d_2Z(t-\tau_2)-\sigma NT$$

$$N^*=\frac{DN_0+m_1d_1P(t-\tau_1)+m_2d_2Z(t-\tau_2)}{D+\alpha P+\sigma T} \tag{5.3}$$

From (4.7), we have;

$$Z\left(\frac{k_2\beta P}{a+P}-\frac{k_3\beta P(t-\tau_3)}{a+P(t-\tau_3)}-(D+d_2)-\varepsilon T-\phi G\right)=0$$

Since $Z\neq 0$,

$$\frac{k_2\beta P}{a+P}-\frac{k_3\beta P(t-\tau_3)}{a+P(t-\tau_3)}-(D+d_2)-\varepsilon T-\phi G=0 \tag{5.4}$$

We substitute (5.2) into (5.4) to solve for Z

$$\frac{k_2\beta P}{a+P}-\frac{k_3\beta P(t-\tau_3)}{a+P(t-\tau_3)}-(D+d_2)-\varepsilon T-\frac{\phi fN}{\theta_2-\phi Z}=0$$

$$Z^*=\frac{\theta_2}{\phi}-\frac{fN(a+P)(a+P(t-\tau_3))}{k_2\beta P-k_3\beta P(t-\tau_3)-(D+d_2+\varepsilon T)(a+P)(a+P(t-\tau_3))} \tag{5.5}$$

from (4.8)

$$O^*=\frac{\psi P}{\mu T+\delta w+\pi_1P+\pi_2Z+\pi_3G} \tag{5.6}$$

and from (4.9), we have;

$$\left(k_1\alpha N-D-d_1-\frac{\beta Z}{a+P}-vP+\pi_1O-hT\right)P=0$$

Since $P\neq 0$, we have;

$$k_1\alpha N-D-d_1-\frac{\beta Z}{a+P}-vP+\pi_1O-hT=0$$

Let $C=k_1\alpha N-D-d_1+\pi_1O-hT$, so that

$$C-\frac{\beta Z}{a+P}-vP=0$$

$$C(a+P)-vP(a+P)-\beta Z=0$$

$$(C-vP)(a+P)-\beta Z=0$$

Expanding, we have;

$$(C-vP)(a+P)-\beta Z=0$$

$$vP^2+(av-C)P+\beta Z-aC=0$$

Solve using the quadratic formula, we have;

$$P=\frac{-(av-C)\pm\sqrt{(av-C)^2-4v(\beta Z-aC)}}{2v}$$

Simplifying the discriminant, we have;

$$(av-C)^2-4v(\beta Z-C)=a^2v^2-2avC+C^2-4v\beta Z+4avC$$

$$=a^2v^2-2avC+C^2-4v\beta Z+4avC$$
$$=a^2v^2+2avC+C^2-4v\beta Z$$
$$=(av+C)^2-4v\beta Z$$

Thus;

$$P=\frac{-(av-C)\pm\sqrt{(av+C)^2-4v\beta Z}}{2v}$$

We recall that $C=k_1\alpha N-D-d_1+\pi_1 O-hT$.

Thus;

$$P^*=\frac{-(av-k_1\alpha N+D+d_1-\pi_1 O+hT)\pm\sqrt{(av+k_1\alpha N-D-d_1+\pi_1 O-hT)^2-4v\beta Z}}{2v}$$

(5.7)

From (5.0), we have;

$$T(\theta_1 G+\sigma N-x+\varepsilon Z)=0$$

Since $T\neq 0$

$$\theta_1 G+\sigma N-x+\varepsilon Z=0 \qquad (5.8)$$

We substitute (5.3) into (5.8) to solve for T

$$\theta_1 G+\frac{\sigma DN_0+m_1d_1P(t-\tau_1)+m_2d_2Z(t-\tau_2)}{D+\alpha P+\sigma T}-x+\varepsilon Z=0$$

$$\sigma T=\frac{\sigma DN_0+m_1d_1P(t-\tau_1)+m_2d_2Z(t-\tau_2)}{x-\varepsilon Z-\theta_1 G}-D-\alpha P$$

$$T^*=\frac{1}{\sigma}\left(\frac{\sigma DN_0+m_1d_1P(t-\tau_1)+m_2d_2Z(t-\tau_2)}{x-\varepsilon Z-\theta_1 G}-D-\alpha P\right) \qquad (5.9)$$

Thus, the coexistence equilibrium point is $E_0=(N^*,Z^*,O^*,P^*,T^*,G^*)$, which imply that;

$$E_0=\left(\begin{array}{c}\frac{DN_0+m_1d_1P(t-\tau_1)+m_2d_2Z(t-\tau_2)}{D+\alpha P+\sigma T},\\ \frac{\theta_2}{\phi}-\frac{fN(a+P)(a+P(t-\tau_3))}{k_2\beta P-k_3\beta P(t-\tau_3)-(D+d_2+\varepsilon T)(a+P)(a+P(t-\tau_3))},\\ \frac{\psi P}{\mu T+\delta w+\pi_1 P+\pi_2 Z+\pi_3 G},\\ \frac{-(av-k_1\alpha N+D+d_1-\pi_1 O+hT)\pm\sqrt{(av+k_1\alpha N-D-d_1+\pi_1 O-hT)^2-4v\beta Z}}{2v},\\ \frac{1}{\sigma}\left(\frac{\sigma DN_0+m_1d_1P(t-\tau_1)+m_2d_2Z(t-\tau_2)}{x-\varepsilon Z-\theta_1 G}-D-\alpha P\right),\frac{fN}{\theta_2-\phi Z}\end{array}\right)$$

7.2 The Existence of Equilibrium Points at Temperature of the Upper Ocean, $T=0^oC$

The freezing temperature of the ocean is approximately -1.9^0C (Olson *et al.,* 2022). Therefore, if $T=0$, then;

the nutrient equation (5.3) becomes;

$$N^*=\frac{DN_0+m_1d_1P(t-\tau_1)+m_2d_2Z(t-\tau_2)}{D+\alpha P} \qquad (6.0)$$

the phytoplankton equation (5.7) becomes;

$$P^*=\frac{-(av-k_1\alpha N+D+d_1-\pi_1 O)\pm\sqrt{(av+k_1\alpha N-D-d_1+\pi_1 O)^2-4v\beta Z}}{2v} \qquad (6.1)$$

The Oxygen equation (5.6) becomes;

$$O^*=\frac{\psi P}{\delta w+\pi_1 P+\pi_2 Z+\pi_3 G}. \qquad (6.2)$$

© JUL 2026 | IRE Journals | Volume 10 Issue 1 | ISSN: 2456-8880
DOI: https://doi.org/10.64388/IREV10I1-1719581

the zooplankton equation (5.5) becomes;

$$Z^* = \frac{\theta_2}{\phi} - \frac{fN\left(a+P\right)\left(a+P(t-\tau_3)\right)}{k_2\beta P - k_3\beta P(t-\tau_3) - \left(D+d_2\right)\left(a+P\right)\left(a+P(t-\tau_3)\right)} \tag{6.3}$$

The greenhouse equation (5.2) remains the same at $T = 0$.

Thus, this gives the equilibrium point $E_1 = \left(N^*, Z^*, \mathrm{O}, \mathrm{P}, 0, G^*\right)$, which imply that;

$$E_1 = \begin{pmatrix} \dfrac{DN_0 + m_1 d_1 P(t-\tau_1) + m_2 d_2 Z(t-\tau_2)}{D+\alpha P}, \dfrac{\theta_2}{\phi} - \dfrac{fN\left(a+P\right)\left(a+P(t-\tau_3)\right)}{k_2\beta P - k_3\beta P(t-\tau_3) - \left(D+d_2\right)\left(a+P\right)\left(a+P(t-\tau_3)\right)}, \\ \dfrac{\psi P}{\delta w + \pi_1 P + \pi_2 Z + \pi_3 G}, \dfrac{-\left(av - k_1\alpha N + D + d_1 - \pi_1 O\right) \pm \sqrt{\left(av + k_1\alpha N - D - d_1 + \pi_1 O\right)^2 - 4v\beta Z}}{2v}, \\ 0, \dfrac{fN}{\theta_2 - \phi Z} \end{pmatrix}$$

VIII. STABILITY ANALYSIS

In this section, we will carry out different stability analysis of the equilibrium points of the system of equation (3.6). Firstly, we will carry out local stability analysis of the coexistence equilibrium points. Secondly, the local stability analysis of equilibrium points at temperature of the upper ocean $T = 0^{\circ}C$.

8.1 Local Stability Analysis of The Coexistence Equilibrium Point

The local stability of the coexistence equilibrium points is analyzed using the method of linearization. We maintain the variables define in (3.6), and the corresponding Jacobian matrix of the system is obtained as:

$$J = \begin{pmatrix} \frac{\partial g_1}{\partial N} & \frac{\partial g_1}{\partial Z} & \frac{\partial g_1}{\partial O} & \frac{\partial g_1}{\partial P} & \frac{\partial g_1}{\partial T} & \frac{\partial g_1}{\partial G} \\ \frac{\partial g_2}{\partial N} & \frac{\partial g_2}{\partial Z} & \frac{\partial g_2}{\partial O} & \frac{\partial g_2}{\partial P} & \frac{\partial g_2}{\partial T} & \frac{\partial g_2}{\partial G} \\ \frac{\partial g_3}{\partial N} & \frac{\partial g_3}{\partial Z} & \frac{\partial g_3}{\partial O} & \frac{\partial g_3}{\partial P} & \frac{\partial g_3}{\partial T} & \frac{\partial g_3}{\partial G} \\ \frac{\partial g_4}{\partial N} & \frac{\partial g_4}{\partial Z} & \frac{\partial g_4}{\partial O} & \frac{\partial g_4}{\partial P} & \frac{\partial g_4}{\partial T} & \frac{\partial g_4}{\partial G} \\ \frac{\partial g_5}{\partial N} & \frac{\partial g_5}{\partial Z} & \frac{\partial g_5}{\partial O} & \frac{\partial g_5}{\partial P} & \frac{\partial g_5}{\partial T} & \frac{\partial g_5}{\partial G} \\ \frac{\partial g_6}{\partial N} & \frac{\partial g_6}{\partial Z} & \frac{\partial g_6}{\partial O} & \frac{\partial g_6}{\partial P} & \frac{\partial g_6}{\partial T} & \frac{\partial g_6}{\partial G} \end{pmatrix} \tag{6.5}$$

Therefore, the Jacobian matrix J is given by

$$J = \begin{pmatrix} S_1 & 0 & 0 & -\alpha N & -\sigma N & 0 \\ 0 & S_2 & 0 & S_3 & -\varepsilon Z & -\phi Z \\ 0 & -\pi_2 O & S_4 & \psi - \pi_1 O & -\mu O & -\pi_3 O \\ k_1\alpha P & S_5 & \pi_1 P & S_6 & -hP & 0 \\ \sigma T & \varepsilon T & 0 & 0 & S_7 & \theta_1 T \\ f & \phi G & 0 & 0 & 0 & S_8 \end{pmatrix} \tag{6.6}$$

Where;

$$S_1 = -D - \alpha P - \sigma T$$

$$S_2 = \frac{k_2\beta P}{a+P} - \frac{k_3\beta P(\mathrm{t}-\tau_3)}{a+P(\mathrm{t}-\tau_3)} - (D+d_2) - \varepsilon T - \phi G$$

$$S_3 = \frac{k_2\beta Z a}{(a+P)^2}$$

$$S_4 = -\mu T - \delta w - \pi_1 P - \pi_2 Z - \pi_3 G$$

$$S_5 = -\frac{\beta P}{a+P}$$

$$S_6 = k_1\alpha N - (D+d_1) - \frac{\beta Z a}{(a+P)^2} - 2vP - hT + \pi_1 O$$

$$S_7 = \theta_1 G + \sigma N - x + \varepsilon Z$$

$$S_8 = -\theta_2 + \phi Z$$

And

© JUL 2026 | IRE Journals | Volume 10 Issue 1 | ISSN: 2456-8880
DOI: https://doi.org/10.64388/IREV10I1-1719581

$$J(E_0)=\begin{pmatrix} A_1 & 0 & 0 & -A_2 & -A_3 & 0 \\ 0 & A_4 & 0 & A_5 & -A_6 & -A_7 \\ 0 & -A_8 & A_9 & A_{10} & -A_{11} & -A_{12} \\ A_{13} & A_{14} & A_{15} & A_{16} & -A_{17} & 0 \\ A_{18} & A_{19} & 0 & 0 & A_{20} & A_{21} \\ f & A_{22} & 0 & 0 & 0 & A_{23} \end{pmatrix} \tag{6.7}$$

Where;

$$A_1=-D+\alpha\left(\frac{av-k_1\alpha N+D+d_1-\pi_1 O+hT\pm\sqrt{\left(av+k_1\alpha N-D-d_1+\pi_1 O-hT\right)^2-4v\beta Z}}{2v}\right)$$

$$-\left(\frac{\sigma DN_0+m_1d_1P(t-\tau_1)+m_2d_2Z(t-\tau_2)}{x-\varepsilon Z-\theta_1 G}-D-\alpha P\right)$$

$$A_2=\frac{\alpha\left(DN_0+m_1d_1P(t-\tau_1)+m_2d_2Z(t-\tau_2)\right)}{D+\alpha P+\sigma T}$$

$$A_3=\frac{\sigma\left(DN_0+m_1d_1P(t-\tau_1)+m_2d_2Z(t-\tau_2)\right)}{D+\alpha P+\sigma T}$$

$$A_4=k_2\beta\left(\frac{-\left(av-k_1\alpha N+D+d_1-\pi_1 O+hT\right)\pm\sqrt{\left(av+k_1\alpha N-D-d_1+\pi_1 O-hT\right)^2-4v\beta Z}}{2av-\left(av-k_1\alpha N+D+d_1-\pi_1 O+hT\right)\pm\sqrt{\left(av+k_1\alpha N-D-d_1+\pi_1 O-hT\right)^2-4v\beta Z}}\right)$$

$$-\frac{k_3\beta P(t-\tau_3)}{a+P(t-\tau_3)}-(D+d_2)-\frac{\varepsilon}{\sigma}\left(\frac{\sigma DN_0+m_1d_1P(t-\tau_1)+m_2d_2Z(t-\tau_2)}{x-\varepsilon Z-\theta_1 G}-D-\alpha P\right)-\frac{\phi fN}{\theta_2-\phi Z}$$

$$A_5=\frac{k_2\beta a\left(\frac{\theta_2}{\phi}-\frac{fN\left(a+P\right)\left(a+P(t-\tau_3)\right)}{k_2\beta P-k_3\beta P(t-\tau_3)-\left(D+d_2+\varepsilon T\right)\left(a+P\right)\left(a+P(t-\tau_3)\right)}\right)}{\left(a+\frac{-\left(av-k_1\alpha N+D+d_1-\pi_1 O+hT\right)\pm\sqrt{\left(av+k_1\alpha N-D-d_1+\pi_1 O-hT\right)^2-4v\beta Z}}{2v}\right)^2}$$

$$A_6=\varepsilon\left(\frac{\theta_2}{\phi}-\frac{fN\left(a+P\right)\left(a+P(t-\tau_3)\right)}{k_2\beta P-k_3\beta P(t-\tau_3)-\left(D+d_2+\varepsilon T\right)\left(a+P\right)\left(a+P(t-\tau_3)\right)}\right)$$

$$A_7=\phi\left(\frac{\theta_2}{\phi}-\frac{fN\left(a+P\right)\left(a+P(t-\tau_3)\right)}{k_2\beta P-k_3\beta P(t-\tau_3)-\left(D+d_2+\varepsilon T\right)\left(a+P\right)\left(a+P(t-\tau_3)\right)}\right)$$

$$A_8=\frac{\pi_2\psi P}{\mu T+\delta w+\pi_1 P+\pi_2 Z+\pi_3 G}$$

$$A_9=-\frac{\mu}{\sigma}\left(\frac{\sigma DN_0+m_1d_1P(t-\tau_1)+m_2d_2Z(t-\tau_2)}{x-\varepsilon Z-\theta_1 G}-D-\alpha P\right)-\delta w-\frac{\pi_3 fN}{\theta_2-\phi Z}$$

$$-\pi_1\left(\frac{-\left(av-k_1\alpha N+D+d_1-\pi_1 O+hT\right)\pm\sqrt{\left(av+k_1\alpha N-D-d_1+\pi_1 O-hT\right)^2-4v\beta Z}}{2v}\right)$$

$$-\pi_2\left(\frac{\theta_2}{\phi}-\frac{fN\left(a+P\right)\left(a+P(t-\tau_3)\right)}{k_2\beta P-k_3\beta P(t-\tau_3)-\left(D+d_2+\varepsilon T\right)\left(a+P\right)\left(a+P(t-\tau_3)\right)}\right)$$

$$A_{10}=\frac{\psi\left(\mu T+\delta w+\pi_2 Z+\pi_3 G\right)}{\mu T+\delta w+\pi_1 P+\pi_2 Z+\pi_3 G},A_{11}=\frac{\mu\psi P}{\mu T+\delta w+\pi_1 P+\pi_2 Z+\pi_3 G}$$

$$A_{12}=\frac{\pi_3\psi P}{\mu T+\delta w+\pi_1 P+\pi_2 Z+\pi_3 G}$$

$$A_{13}=k_1\alpha\left(\frac{-\left(av-k_1\alpha N+D+d_1-\pi_1 O+hT\right)\pm\sqrt{\left(av+k_1\alpha N-D-d_1+\pi_1 O-hT\right)^2-4v\beta Z}}{2v}\right)$$

$$A_{14}=-\beta\left(\frac{-\left(av-k_1\alpha N+D+d_1-\pi_1 O+hT\right)\pm\sqrt{\left(av+k_1\alpha N-D-d_1+\pi_1 O-hT\right)^2-4v\beta Z}}{2av-\left(av-k_1\alpha N+D+d_1-\pi_1 O+hT\right)\pm\sqrt{\left(av+k_1\alpha N-D-d_1+\pi_1 O-hT\right)^2-4v\beta Z}}\right)$$

$$A_{15}=\pi_1\left(\frac{-\left(av-k_1\alpha N+D+d_1-\pi_1 O+hT\right)\pm\sqrt{\left(av+k_1\alpha N-D-d_1+\pi_1 O-hT\right)^2-4v\beta Z}}{2v}\right)$$

$$A_{16}=k_1\alpha\left(\frac{DN_0+m_1d_1P(t-\tau_1)+m_2d_2Z(t-\tau_2)}{D+\alpha P+\sigma T}\right)-(D+d_1)+\frac{\pi_1\psi P}{\mu T+\delta w+\pi_1 P+\pi_2 Z+\pi_3 G}$$

$$-\frac{\beta a\left(\frac{\theta_2}{\phi}-\frac{fN\left(a+P\right)\left(a+P(t-\tau_3)\right)}{k_2\beta P-k_3\beta P(t-\tau_3)-\left(D+d_2+\varepsilon T\right)\left(a+P\right)\left(a+P(t-\tau_3)\right)}\right)}{\left(a+\frac{-\left(av-k_1\alpha N+D+d_1-\pi_1 O+hT\right)\pm\sqrt{\left(av+k_1\alpha N-D-d_1+\pi_1 O-hT\right)^2-4v\beta Z}}{2v}\right)^2}$$

$$+\left(av-k_1\alpha N+D+d_1-\pi_1 O+hT\right)\pm\sqrt{\left(av+k_1\alpha N-D-d_1+\pi_1 O-hT\right)^2-4v\beta Z}$$

$$-\frac{h}{\sigma}\left(\frac{\sigma DN_0+m_1d_1P(t-\tau_1)+m_2d_2Z(t-\tau_2)}{x-\varepsilon Z-\theta_1 G}-D-\alpha P\right)$$

$$A_{17}=h\left(\frac{-\left(av-k_1\alpha N+D+d_1-\pi_1 O+hT\right)\pm\sqrt{\left(av+k_1\alpha N-D-d_1+\pi_1 O-hT\right)^2-4v\beta Z}}{2v}\right)$$

$$A_{18}=\frac{\sigma DN_0+m_1d_1P(t-\tau_1)+m_2d_2Z(t-\tau_2)}{x-\varepsilon Z-\theta_1 G}-D-\alpha P$$

$$A_{19}=\frac{\varepsilon}{\sigma}\left(\frac{\sigma DN_0+m_1d_1P(t-\tau_1)+m_2d_2Z(t-\tau_2)}{x-\varepsilon Z-\theta_1 G}-D-\alpha P\right)$$

$$A_{20}=\varepsilon\left(\frac{\theta_2}{\phi}-\frac{fN\left(a+P\right)\left(a+P(t-\tau_3)\right)}{k_2\beta P-k_3\beta P(t-\tau_3)-\left(D+d_2+\varepsilon T\right)\left(a+P\right)\left(a+P(t-\tau_3)\right)}\right)-x$$

$$+\frac{\theta_1 fN}{\theta_2-\phi Z}+\sigma\left(\frac{DN_0+m_1d_1P(t-\tau_1)+m_2d_2Z(t-\tau_2)}{D+\alpha P+\sigma T}\right)$$

$$A_{21}=\frac{\theta_1}{\sigma}\left(\frac{\sigma DN_0+m_1d_1P(t-\tau_1)+m_2d_2Z(t-\tau_2)}{x-\varepsilon Z-\theta_1 G}-D-\alpha P\right)$$

$$A_{23}=-\theta_2+\phi\left(\frac{\theta_2}{\phi}-\frac{fN\left(a+P\right)\left(a+P(t-\tau_3)\right)}{k_2\beta P-k_3\beta P(t-\tau_3)-\left(D+d_2+\varepsilon T\right)\left(a+P\right)\left(a+P(t-\tau_3)\right)}\right)$$

Thus;

$$\left|J(E_0)-\lambda I\right|=\begin{vmatrix} A_1-\lambda & 0 & 0 & -A_2 & -A_3 & 0 \\ 0 & A_4-\lambda & 0 & A_5 & -A_6 & -A_7 \\ 0 & -A_8 & A_9-\lambda & A_{10} & -A_{11} & -A_{12} \\ A_{13} & A_{14} & A_{15} & A_{16}-\lambda & -A_{17} & 0 \\ A_{18} & A_{19} & 0 & 0 & A_{20}-\lambda & A_{21} \\ f & A_{22} & 0 & 0 & 0 & A_{23}-\lambda \end{vmatrix}=0 \tag{6.8}$$

Using maple to decompose matrix (6.8) into upper triangular matrix, using Gaussian elimination method. We have;

$$\left|J(E_0)-\lambda I\right|=\begin{vmatrix} A_1-\lambda & 0 & 0 & -A_2 & -A_3 & 0 \\ 0 & A_4-\lambda & 0 & A_5 & -A_6 & -A_7 \\ 0 & 0 & A_9-\lambda & A_{10}+\frac{A_5A_8}{A_4-\lambda} & -A_{11}-\frac{A_6A_8}{A_4-\lambda} & -A_{12}-\frac{A_7A_8}{A_4-\lambda} \\ 0 & 0 & 0 & U_{44} & U_{45} & U_{46} \\ 0 & 0 & 0 & 0 & U_{55} & U_{56} \\ 0 & 0 & 0 & 0 & 0 & U_{66} \end{vmatrix}=0 \tag{6.9}$$

Where;

$$U_{66}=A_{23}-\lambda+\frac{A_7A_{22}}{A_4-\lambda}-\frac{C_{64}U_{46}}{U_{44}}-\frac{C_{65}U_{56}}{U_{55}}$$

$$C_{65}=\frac{fA_3}{A_1-\lambda}+\frac{A_6A_{22}}{A_4-\lambda}$$

$$C_{64}=\frac{fA_2}{A_1-\lambda}-\frac{A_5A_{22}}{A_4-\lambda}$$

$$U_{56}=A_{20}+\frac{A_7A_{19}}{A_4-\lambda}-\frac{C_{54}U_{46}}{U_{44}}$$

$$U_{55}=A_{20}-\lambda+\frac{A_3A_{18}}{A_1-\lambda}+\frac{A_6A_{19}}{A_4-\lambda}-\frac{C_{54}U_{45}}{U_{44}}$$

$$C_{54}=\frac{A_2A_{18}}{A_1-\lambda}-\frac{A_5A_{19}}{A_4-\lambda}$$

$$U_{46}=\frac{A_7A_{14}}{A_4-\lambda}-\frac{A_{15}}{A_9-\lambda}\left(A_{12}+\frac{A_7A_8}{A_4-\lambda}\right)$$

$$U_{45}=-A_{17}+\frac{A_3A_{13}}{A_1-\lambda}+\frac{A_6A_{14}}{A_4-\lambda}-\frac{A_{15}}{A_9-\lambda}\left(A_{11}+\frac{A_6A_8}{A_4-\lambda}\right)$$

$$U_{44}=A_{16}-\lambda+\frac{A_2A_{13}}{A_1-\lambda}-\frac{A_5A_{14}}{A_4-\lambda}-\frac{A_{15}}{A_9-\lambda}\left(A_{10}+\frac{A_5A_8}{A_4-\lambda}\right)$$

We extract the diagonal elements from matrix (6.9) as the eigenvalues. The product of the eigenvalues gives the characteristics equation;

$$\lambda^6+a_1\lambda^5+a_2\lambda^4+a_3\lambda^3+a_4\lambda^2+a_5\lambda+a_6=0 \tag{7.0}$$

Where;

$$a_1=A_1+A_4+A_9+A_{16}+A_{20}+A_{23}$$

$$a_2=A_1A_4+A_1A_9+A_4A_9+\left(A_1+A_4+A_9\right)\left(A_{16}+A_{20}+A_{23}\right)+A_{16}A_{20}+A_{16}A_{23}+A_{20}A_{23}-A_{12}A_{13}-A_3A_{18}$$
$$+A_5A_{14}+A_6A_{19}+A_{10}A_{15}$$

$$a_3=-\left(A_1+A_4+A_9\right)\left(A_{16}A_{20}+A_{16}A_{23}+A_{20}A_{23}\right)-\left(A_1A_4+A_1A_9+A_4A_9\right)\left(A_{16}+A_{20}+A_{23}\right)-A_1A_4A_9$$
$$-A_{16}A_{20}A_{23}+A_{23}\left(A_2A_{13}+A_3A_{18}\right)+A_2A_{13}A_{20}+A_3A_{16}A_{18}-A_{23}\left(A_5A_{14}+A_6A_{19}\right)-A_5A_{14}A_{20}-A_6A_{16}A_{19}$$
$$-A_{10}A_{15}A_{23}+A_2A_{17}A_{18}+fA_3A_{21}$$

$$a_4 = A_1A_4A_9\left(A_{16}+A_{20}+A_{23}\right)+\left(A_1A_4+A_1A_9+A_4A_9\right)\left(A_{16}A_{20}+A_{16}A_{23}+A_{20}A_{23}\right)$$
$$+A_{16}A_{20}A_{23}\left(A_1+A_4+A_9\right)-A_1A_3A_4A_{18}-A_1A_2A_9A_{13}-A_2A_4A_9A_{13}+A_1A_4A_6A_{19}+A_1A_5A_9A_{14}$$
$$+A_4A_5A_9A_{14}+A_1A_4A_{10}A_{15}-A_2A_{17}A_{18}A_{23}-fA_3A_{21}A_{23}$$

$$a_5 = -A_1A_4A_9\left(A_{16}A_{20}+A_{16}A_{23}+A_{20}A_{23}\right)-A_{16}A_{20}A_{23}\left(A_1A_4+A_1A_9+A_4A_9\right)+A_1A_3A_4A_{18}A_{23}+A_1A_2A_9A_{13}A_{23}$$
$$-A_1A_4A_6A_{19}A_{23}-A_1A_5A_9A_{14}A_{23}+A_1A_2A_4A_{17}A_{18}+fA_1A_3A_4A_{21}$$

$$a_6 = A_1A_4A_{23}\left(A_9A_{16}A_{20}-A_3A_9A_{10}-A_2A_9A_{13}+A_6A_9A_{19}+A_5A_9A_{14}\right)-A_1A_4A_9\left(A_2A_{17}A_{18}+fA_3A_{21}\right)$$

We adopted Routh- Hurwitz criterion for stability to investigate the stability of (7.0).

For order one;

$$a_0\lambda + a_1 = 0$$

But $a_0 = 1$ in (7.0).

Thus,

$$\Delta_1 = a_1 > 0$$

For order two;

$$a_0\lambda^2 + a_1\lambda + a_2 = 0$$

$$\Delta_2 = \begin{vmatrix} a_1 & 0 \\ 1 & a_2 \end{vmatrix} \Rightarrow \Delta_2 = a_1a_2 > 0$$

For order three;

$$a_0\lambda^3 + a_1\lambda^2 + a_2\lambda + a_3 = 0$$

$$\Delta_3 = \begin{vmatrix} a_1 & a_3 & 0 \\ 1 & a_2 & 0 \\ 0 & a_1 & a_3 \end{vmatrix} \Rightarrow \Delta_3 = a_1a_2a_3 - {a_3}^2 > 0$$

For order four;

$$a_0\lambda^4 + a_1\lambda^3 + a_2\lambda^2 + a_3\lambda + a_4 = 0$$

$$\Delta_4 = \begin{vmatrix} a_1 & a_3 & 0 & 0 \\ 1 & a_2 & a_4 & 0 \\ 0 & a_1 & a_3 & 0 \\ 0 & 1 & a_2 & a_4 \end{vmatrix}$$

This gives,

$$\Delta_1 = a_1, \Delta_2 = \begin{vmatrix} a_1 & a_3 \\ 1 & a_2 \end{vmatrix}, \Delta_3 = \begin{vmatrix} a_1 & a_3 & 0 \\ 1 & a_2 & a_4 \\ 0 & a_1 & a_3 \end{vmatrix} \Rightarrow \Delta_3 = a_1a_2a_3 - a_1^2a_4 - {a_3}^2$$

Thus,

$$\Delta_4 = a_4\Delta_3 = a_4\left(a_1a_2a_3 - a_1^2a_4 - {a_3}^2\right)$$

$$\Delta_4 = a_1a_2a_3a_4 - a_1^2{a_4}^2 - {a_3}^2a_4 > 0$$

For order five;

$$a_0\lambda^5 + a_1\lambda^4 + a_2\lambda^3 + a_3\lambda^2 + a_4\lambda + a_5 = 0$$

$$\Delta_5 = \begin{vmatrix} a_1 & a_3 & a_5 & 0 & 0 \\ 1 & a_2 & a_4 & 0 & 0 \\ 0 & a_1 & a_3 & a_5 & 0 \\ 0 & 1 & a_2 & a_4 & 0 \\ 0 & 0 & a_1 & a_3 & a_5 \end{vmatrix}$$

This gives,

$$\Delta_1 = a_1, \Delta_2 = \begin{vmatrix} a_1 & a_3 \\ 1 & a_2 \end{vmatrix}, \Delta_3 = \begin{vmatrix} a_1 & a_3 & a_5 \\ 1 & a_2 & a_4 \\ 0 & a_1 & a_3 \end{vmatrix} \Rightarrow \Delta_3 = a_1a_2a_3 - a_1^2a_4 - {a_3}^2 + a_1a_5,$$

$$\Delta_4 = \begin{vmatrix} a_1 & a_3 & a_5 & 0 \\ 1 & a_2 & a_4 & 0 \\ 0 & a_1 & a_3 & a_5 \\ 0 & 1 & a_2 & a_4 \end{vmatrix} \Rightarrow a_5\begin{vmatrix} a_1 & a_3 & a_5 \\ 1 & a_2 & a_4 \\ 0 & 1 & a_2 \end{vmatrix} - a_4\begin{vmatrix} a_1 & a_3 & a_5 \\ 1 & a_2 & a_4 \\ 0 & a_1 & a_3 \end{vmatrix}$$

$$\Delta_4 = a_5\left[a_1\left(a_2^2 - a_4\right) - a_3\left(a_2\right) + a_5\right] - a_4\left[a_1\left(a_2a_3 - a_1a_4\right) - {a_3}^2 + a_1a_5\right]$$

$$\Delta_4 = a_1a_2^2a_5 - a_1a_4a_5 - a_2a_3a_5 + {a_5}^2 - a_1a_2a_3a_4 + a_1^2{a_4}^2 + {a_3}^2a_4 - a_1a_4a_5$$

Thus,

$$\Delta_5 = a_5\Delta_4 = a_5\left(a_1a_2^2a_5 - 2a_1a_4a_5 - a_2a_3a_5 + {a_5}^2 - a_1a_2a_3a_4 + a_1^2{a_4}^2 + {a_3}^2a_4\right)$$

$$\Delta_5 = a_1a_2^2{a_5}^2 - 2a_1a_4{a_5}^2 - a_2a_3{a_5}^2 + {a_5}^3 - a_1a_2a_3a_4a_5 + a_1^2{a_4}^2a_5 + {a_3}^2a_4a_5 > 0$$

For order six;

$$a_0\lambda^6 + a_1\lambda^5 + a_2\lambda^4 + a_3\lambda^3 + a_4\lambda^2 + a_5\lambda + a_6 = 0$$

$$\Delta_6 = \begin{vmatrix} a_1 & a_3 & a_5 & 0 & 0 & 0 \\ 1 & a_2 & a_4 & a_6 & 0 & 0 \\ 0 & a_1 & a_3 & a_5 & 0 & 0 \\ 0 & 1 & a_2 & a_4 & a_6 & 0 \\ 0 & 0 & a_1 & a_3 & a_5 & 0 \\ 0 & 0 & 1 & a_2 & a_4 & a_6 \end{vmatrix}$$

This gives,

$$\Delta_1 = a_1, \Delta_2 = \begin{vmatrix} a_1 & a_3 \\ 1 & a_2 \end{vmatrix}, \Delta_3 = \begin{vmatrix} a_1 & a_3 & a_5 \\ 1 & a_2 & a_4 \\ 0 & a_1 & a_3 \end{vmatrix} \Rightarrow \Delta_3 = a_1a_2a_3 - a_1^2a_4 - a_3^2 + a_1a_5,$$

$$\Delta_4 = \begin{vmatrix} a_1 & a_3 & a_5 & 0 \\ 1 & a_2 & a_4 & a_6 \\ 0 & a_1 & a_3 & a_5 \\ 0 & 1 & a_2 & a_4 \end{vmatrix} \Rightarrow -a_6 \begin{vmatrix} a_1 & a_3 & a_5 \\ 0 & a_1 & a_3 \\ 0 & 1 & a_2 \end{vmatrix} + a_5 \begin{vmatrix} a_1 & a_3 & a_5 \\ 1 & a_2 & a_4 \\ 0 & 1 & a_2 \end{vmatrix} - a_4 \begin{vmatrix} a_1 & a_3 & a_5 \\ 1 & a_2 & a_4 \\ 0 & a_1 & a_3 \end{vmatrix}$$

$$\Delta_4 = -a_6\left[a_1\left(a_1a_2 - a_3\right)\right] + a_5\left[a_1\left(a_2^2 - a_4\right) - a_3\left(a_2\right) + a_5\right] - a_4\left[a_1\left(a_2a_3 - a_1a_4\right) - a_3^2 + a_1a_5\right]$$

$$\Delta_4 = a_1a_3a_6 + a_1a_2^2a_5 - 2a_1a_4a_5 - a_2a_3a_5 + a_5^2 - a_1a_2a_3a_4 + a_1^2a_4^2 + a_3^2a_4 - a_1^2a_2a_6,$$

$$\Delta_5 = \begin{vmatrix} a_1 & a_3 & a_5 & 0 & 0 \\ 1 & a_2 & a_4 & a_6 & 0 \\ 0 & a_1 & a_3 & a_5 & 0 \\ 0 & 1 & a_2 & a_4 & a_6 \\ 0 & 0 & a_1 & a_3 & a_5 \end{vmatrix} \Rightarrow -a_6 \begin{vmatrix} a_1 & a_3 & a_5 & 0 \\ 1 & a_2 & a_4 & a_6 \\ 0 & a_1 & a_3 & a_5 \\ 0 & 0 & a_1 & a_3 \end{vmatrix} + a_5 \begin{vmatrix} a_1 & a_3 & a_5 & 0 \\ 1 & a_2 & a_4 & a_6 \\ 0 & a_1 & a_3 & a_5 \\ 0 & 1 & a_2 & a_4 \end{vmatrix}$$

$$\Delta_5 = -a_6\left[\begin{vmatrix} a_1 & a_3 & a_5 \\ -a_6 & a_1 & a_3 \\ 0 & 0 & a_1 \end{vmatrix} + a_5 \begin{vmatrix} a_1 & a_3 & a_5 \\ 1 & a_2 & a_4 \\ 0 & 0 & a_1 \end{vmatrix} - a_3 \begin{vmatrix} a_1 & a_3 & a_5 \\ 1 & a_2 & a_4 \\ 0 & a_1 & a_3 \end{vmatrix}\right] + a_5\Delta_4$$

$$\Delta_5 = -a_6\left[-a_6\left(a_1^3\right) + a_5\left(a_1\left(a_1a_2\right) - a_1a_3\right) - a_3\left(a_1\left(a_2a_3 - a_1a_4\right)\right)\right] + a_5\Delta_4$$

$$\Delta_5 = -a_6\left(-a_1^3a_6 + a_1^2a_2a_5 - a_1a_3a_5 - a_1a_2a_3^2 + a_1a_3a_4\right) + a_5\Delta_4$$

$$\Delta_5 = a_1^3a_6^2 - 2a_1^2a_2a_5a_6 + 2a_1a_3a_5a_6 + a_1a_2a_3^2a_6 - a_1a_3a_4a_6 + a_1a_2^2a_5^2 - 2a_1a_4a_5^2 - a_2a_3a_5^2 + a_5^3$$
$$-a_1a_2a_3a_4a_5 + a_1^2a_4^2a_5 + a_3^2a_4a_5,$$

$$\Delta_6 = \begin{vmatrix} a_1 & a_3 & a_5 & 0 & 0 & 0 \\ 1 & a_2 & a_4 & a_6 & 0 & 0 \\ 0 & a_1 & a_3 & a_5 & 0 & 0 \\ 0 & 1 & a_2 & a_4 & a_6 & 0 \\ 0 & 0 & a_1 & a_3 & a_5 & 0 \\ 0 & 0 & 1 & a_2 & a_4 & a_6 \end{vmatrix} = a_6\Delta_5$$

$$\Delta_6 = a_6\begin{pmatrix} a_1^3a_6^2 - 2a_1^2a_2a_5a_6 + 2a_1a_3a_5a_6 + a_1a_2a_3^2a_6 - a_1a_3a_4a_6 + a_1a_2^2a_5^2 - 2a_1a_4a_5^2 - a_2a_3a_5^2 + a_5^3 \\ -a_1a_2a_3a_4a_5 + a_1^2a_4^2a_5 + a_3^2a_4a_5 \end{pmatrix}$$

$$\Delta_6 = a_1^3a_6^3 - 2a_1^2a_2a_5a_6^2 + 2a_1a_3a_5a_6^2 + a_1a_2a_3^2a_6^2 - a_1a_3a_4a_6^2 + a_1a_2^2a_5^2a_6 - 2a_1a_4a_5^2a_6 - a_2a_3a_5^2a_6$$
$$+a_5^3a_6 - a_1a_2a_3a_4a_5a_6 + a_1^2a_4^2a_5a_6 + a_3^2a_4a_5a_6 > 0$$

Thus, by Routh Hurwitz criteria, the determinant of equation (7.0) is given by;

$$a_1^3a_6^3 - 2a_1^2a_2a_5a_6^2 + 2a_1a_3a_5a_6^2 + a_1a_2a_3^2a_6^2 - a_1a_3a_4a_6^2 + a_1a_2^2a_5^2a_6 - 2a_1a_4a_5^2a_6 - a_2a_3a_5^2a_6$$
$$+a_5^3a_6 - a_1a_2a_3a_4a_5a_6 + a_1^2a_4^2a_5a_6 + a_3^2a_4a_5a_6$$

The roots $\lambda_1, \lambda_2, \lambda_3, \lambda_4, \lambda_5,$ and λ_6 will have negative real parts provided that;

$$\begin{pmatrix} a_1^3a_6^3 + 2a_1a_3a_5a_6^2 + a_1a_2a_3^2a_6^2 + a_1a_2^2a_5^2a_6 + a_5^3a_6 \\ +a_1^2a_4^2a_5a_6 + a_3^2a_4a_5a_6 \end{pmatrix} > \begin{pmatrix} 2a_1^2a_2a_5a_6^2 + a_1a_2a_4a_6^2 + 2a_1a_4a_5^2a_6 \\ +a_2a_3a_5^2a_6 + a_1a_2a_3a_4a_5a_6 \end{pmatrix}$$

(Routh Hurwitz criteria) holds. Therefore, the coexistence equilibrium point, $E_0 = \left(N^*, Z^*, O^*, P^*, T^*, G^*\right)$ is locally asymptotically stable.

8.2 Local Stability Analysis of Equilibrium Points at Temperature of the Upper Ocean, $T = 0^oC$

The local stability of the equilibrium points at temperature of the upper Ocean, $T = 0$ is analyzed using the method of linearization. Again, maintain the variables define in (3.6), and the corresponding Jacobian matrix of the system is obtained as:

$$J = \begin{pmatrix} \frac{\partial g_1}{\partial N} & \frac{\partial g_1}{\partial Z} & \frac{\partial g_1}{\partial O} & \frac{\partial g_1}{\partial P} & \frac{\partial g_1}{\partial G} \\ \frac{\partial g_2}{\partial N} & \frac{\partial g_2}{\partial Z} & \frac{\partial g_2}{\partial O} & \frac{\partial g_2}{\partial P} & \frac{\partial g_2}{\partial G} \\ \frac{\partial g_3}{\partial N} & \frac{\partial g_3}{\partial Z} & \frac{\partial g_3}{\partial O} & \frac{\partial g_3}{\partial P} & \frac{\partial g_3}{\partial G} \\ \frac{\partial g_4}{\partial N} & \frac{\partial g_4}{\partial Z} & \frac{\partial g_4}{\partial O} & \frac{\partial g_4}{\partial P} & \frac{\partial g_4}{\partial G} \\ \frac{\partial g_6}{\partial N} & \frac{\partial g_6}{\partial Z} & \frac{\partial g_6}{\partial O} & \frac{\partial g_6}{\partial P} & \frac{\partial g_6}{\partial G} \end{pmatrix} \tag{7.1}$$

This Jacobian matrix J is given by

© JUL 2026 | IRE Journals | Volume 10 Issue 1 | ISSN: 2456-8880
DOI: https://doi.org/10.64388/IREV10I1-1719581

$$J=\begin{pmatrix} L_1 & 0 & 0 & -\alpha N & 0 \\ 0 & L_2 & 0 & L_3 & -\phi Z \\ 0 & -\pi_2 O & L_4 & \psi-\pi_1 O & -\pi_3 O \\ k_1\alpha P & L_5 & \pi_1 P & L_6 & 0 \\ f & \phi G & 0 & 0 & L_7 \end{pmatrix} \tag{7.2}$$

Where;

$$L_1=-D-\alpha P$$

$$L_2=\frac{k_2\beta P}{a+P}-\frac{k_3\beta P(\mathrm{t}-\tau_3)}{a+P(\mathrm{t}-\tau_3)}-(D+d_2)-\phi G$$

$$L_3=\frac{k_2\beta Z a}{(a+P)^2}$$

$$L_4=-\delta w-\pi_1 P-\pi_2 Z-\pi_3 G$$

$$L_5=-\frac{\beta P}{a+P}$$

$$L_6=k_1\alpha N-(D+d_1)-\frac{\beta Z a}{(a+P)^2}-2vP+\pi_1 O$$

$$L_7=-\theta_2+\phi Z$$

And

$$J(E_1)=\begin{pmatrix} B_1 & 0 & 0 & -B_2 & 0 \\ 0 & B_3 & 0 & B_4 & -B_5 \\ 0 & -B_6 & B_7 & B_8 & -B_9 \\ B_{10} & B_{11} & B_{12} & B_{13} & 0 \\ f & B_{14} & 0 & 0 & B_{15} \end{pmatrix}=0 \tag{7.3}$$

Where;

$$B_1=-D-\alpha\left(\frac{-\left(av-k_1\alpha N+D+d_1-\pi_1 O\right)\pm\sqrt{\left(av+k_1\alpha N-D-d_1+\pi_1 O\right)^2-4v\beta Z}}{2v}\right)$$

$$B_2=\alpha\left(\frac{DN_0+m_1d_1P(t-\tau_1)+m_2d_2Z(t-\tau_2)}{D+\alpha P}\right)$$

$$B_3=k_2\beta\left(\frac{-\left(av-k_1\alpha N+D+d_1-\pi_1 O\right)\pm\sqrt{\left(av-k_1\alpha N+D+d_1-\pi_1 O\right)^2-4v\left(\beta Z-a\left(k_1\alpha N-D-d_1+\pi_1 O\right)\right)}}{2av-\left(av-k_1\alpha N+D+d_1-\pi_1 O\right)\pm\sqrt{\left(av-k_1\alpha N+D+d_1-\pi_1 O\right)^2-4v\left(\beta Z-a\left(k_1\alpha N-D-d_1+\pi_1 O\right)\right)}}\right)-(D+d_2)-\frac{\phi fN}{\theta_2-\phi Z}$$

$$-\frac{k_3\beta P(\mathrm{t}-\tau_3)}{a+P(\mathrm{t}-\tau_3)}$$

$$B_4=\frac{k_2\beta a\left(\frac{\theta_2}{\phi}-\frac{fN(a+P)(a+P(t-\tau_3))}{k_2\beta P-k_3\beta P(t-\tau_3)-(D+d_2)(a+P)(a+P(t-\tau_3))}\right)}{\left(a+\frac{-\left(av-k_1\alpha N+D+d_1-\pi_1 O\right)\pm\sqrt{\left(av+k_1\alpha N-D-d_1+\pi_1 O\right)^2-4v\beta Z}}{2v}\right)^2}$$

$$B_5=\theta_2-\frac{\phi fN(a+P)(a+P(t-\tau_3))}{k_2\beta P-k_3\beta P(t-\tau_3)-(D+d_2)(a+P)(a+P(t-\tau_3))}$$

$$B_6=\frac{\pi_2\psi P}{\delta w+\pi_1 P+\pi_2 Z+\pi_3 G}$$

$$B_7=-\delta w-\pi_1\left(\frac{-\left(av-k_1\alpha N+D+d_1-\pi_1 O\right)\pm\sqrt{\left(av+k_1\alpha N-D-d_1+\pi_1 O\right)^2-4v\beta Z}}{2v}\right)$$

$$-\pi_2\left(\frac{\theta_2}{\phi}-\frac{fN(a+P)(a+P(t-\tau_3))}{k_2\beta P-k_3\beta P(t-\tau_3)-(D+d_2)(a+P)(a+P(t-\tau_3))}\right)-\frac{\pi_3 fN}{\theta_2-\phi Z}$$

$$B_8=\psi-\frac{\pi_1\psi P}{\delta w+\pi_1 P+\pi_2 Z+\pi_3 G},\ B_9=\frac{\pi_3\psi P}{\delta w+\pi_1 P+\pi_2 Z+\pi_3 G}$$

$$B_{10}=k_1\alpha\left(\frac{-\left(av-k_1\alpha N+D+d_1-\pi_1 O\right)\pm\sqrt{\left(av+k_1\alpha N-D-d_1+\pi_1 O\right)^2-4v\beta Z}}{2v}\right)$$

$$B_{11}=-\beta\left(\frac{-\left(av-k_1\alpha N+D+d_1-\pi_1 O\right)\pm\sqrt{\left(av+k_1\alpha N-D-d_1+\pi_1 O\right)^2-4v\beta Z}}{2av-\left(av-k_1\alpha N+D+d_1-\pi_1 O\right)\pm\sqrt{\left(av+k_1\alpha N-D-d_1+\pi_1 O\right)^2-4v\beta Z}}\right)$$

$$B_{12}=\pi_1\left(\frac{-\left(av-k_1\alpha N+D+d_1-\pi_1 O\right)\pm\sqrt{\left(av+k_1\alpha N-D-d_1+\pi_1 O\right)^2-4v\beta Z}}{2v}\right)$$

$$B_{13}=k_1\alpha\left(\frac{DN_0+m_1d_1P(t-\tau_1)+m_2d_2Z(t-\tau_2)}{D+\alpha P}\right)-(D+d_1)+\frac{\pi_1\psi P}{\delta w+\pi_1 P+\pi_2 Z+\pi_3 G}$$

$$-\frac{\beta a\left(\frac{\theta_2}{\phi}-\frac{fN(a+P)(a+P(t-\tau_3))}{k_2\beta P-k_3\beta P(t-\tau_3)-(D+d_2)(a+P)(a+P(t-\tau_3))}\right)}{\left(a+\frac{-\left(av-k_1\alpha N+D+d_1-\pi_1 O\right)\pm\sqrt{\left(av+k_1\alpha N-D-d_1+\pi_1 O\right)^2-4v\beta Z}}{2v}\right)^2}$$

$$+av-k_1\alpha N+D+d_1-\pi_1 O\pm\sqrt{\left(av+k_1\alpha N-D-d_1+\pi_1 O\right)^2-4v\beta Z}$$

© JUL 2026 | IRE Journals | Volume 10 Issue 1 | ISSN: 2456-8880
DOI: https://doi.org/10.64388/IREV10I1-1719581

$$B_{14}=\frac{\phi fN}{\theta_2-\phi Z}$$

$$B_{15}=-\theta_2+\theta_2-\frac{\phi fN\left(a+P\right)\left(a+P(t-\tau_3)\right)}{k_2\beta P-k_3\beta P(t-\tau_3)-\left(D+d_2\right)\left(a+P\right)\left(a+P(t-\tau_3)\right)}$$

Thus;

$$\left|J(E_1)-\lambda I\right|=\begin{vmatrix} B_1-\lambda & 0 & 0 & -B_2 & 0 \\ 0 & B_3-\lambda & 0 & B_4 & -B_5 \\ 0 & -B_6 & B_7-\lambda & B_8 & -B_9 \\ B_{10} & B_{11} & B_{12} & B_{13}-\lambda & 0 \\ f & B_{14} & 0 & 0 & B_{15}-\lambda \end{vmatrix}=0 \quad (7.4)$$

Using maple to decompose matrix (7.4) into upper triangular matrix, using Gaussian elimination method. We have;

$$\left|J(E_1)-\lambda I\right|=\begin{vmatrix} B_1-\lambda & 0 & 0 & -B_2 & 0 \\ 0 & B_3-\lambda & 0 & B_4 & -B_5 \\ 0 & 0 & B_7-\lambda & B_8+\frac{B_6B_4}{B_3-\lambda} & -B_9-\frac{B_6B_5}{B_3-\lambda} \\ 0 & 0 & 0 & Q_{44} & Q_{45} \\ 0 & 0 & 0 & 0 & Q_{55} \end{vmatrix}=0 \quad (7.5)$$

Where;

$$Q_{44}=B_{13}-\lambda-\frac{B_2B_{10}}{B_1-\lambda}-\frac{B_4B_{11}}{B_3-\lambda}-\frac{B_8B_{12}}{B_7-\lambda}-\frac{B_4B_6B_{12}}{\left(B_3-\lambda\right)\left(B_7-\lambda\right)}$$

$$Q_{45}=\frac{B_5B_{11}}{B_3-\lambda}-\frac{B_9B_{12}}{B_7-\lambda}-\frac{B_5B_6B_{12}}{\left(B_3-\lambda\right)\left(B_7-\lambda\right)}$$

$$Q_{54}=\frac{fB_2}{B_1-\lambda}-\frac{B_4B_{14}}{B_3-\lambda}$$

$$Q_{55}=B_{15}-\lambda-\frac{B_5B_{14}}{B_3-\lambda}-\frac{Q_{54}Q_{45}}{Q_{44}}$$

Similarly, the diagonal elements from matrix (7.5) are the eigenvalues. The product of the eigenvalues gives the characteristics equation;

$$\lambda^5+b_1\lambda^4+b_2\lambda^3+b_3\lambda^2+b_4\lambda+b_5=0 \quad (7.6)$$

Where;

$$b_1=-\left(B_1+B_3+B_7+B_{13}+B_{15}\right)$$

$$b_2=B_1\left(B_3+B_7+B_{13}+B_{15}\right)-B_2B_{10}-B_4B_{11}-B_8B_{12}+B_{13}\left(B_3+B_7+B_{15}\right)-B_5B_{14}+B_{15}\left(B_3+B_7\right)+B_3B_7$$

$$b_3=B_1\left(B_4B_{11}+B_8B_{12}\right)-B_1B_{13}\left(B_3+B_7+B_{15}\right)+B_1\left(B_5B_{14}-B_3B_7\right)-B_1B_{15}\left(B_3+B_7\right)+B_2B_{10}\left(B_3+B_7+B_{15}\right)$$
$$B_4B_{11}\left(B_7+B_{15}\right)+B_{12}\left(B_3B_8+B_4B_6+B_8B_{15}\right)+B_{13}\left(B_5B_{14}-B_3B_7-B_3B_{15}-B_7B_{15}\right)+B_7\left(B_5B_{14}-B_3B_{15}\right)$$

$$b_4=-B_1B_4B_{11}\left(B_7+B_{15}\right)-B_1B_{12}\left(B_3B_8+B_4B_6+B_8B_{15}\right)+B_1B_{13}\left(B_3B_7+B_3B_{15}-B_5B_{14}+B_7B_{15}\right)$$
$$+B_1B_7\left(B_3B_{15}-B_5B_{14}\right)-B_2B_{10}\left(B_5B_{11}+B_9B_{12}+B_3B_{15}+B_7B_{15}+B_3B_7-B_5B_{14}\right)-B_4B_7B_{11}B_{15}$$
$$+B_{12}B_{14}\left(B_3B_8-B_4B_9\right)-B_{12}B_{15}\left(B_3B_8+B_4B_6\right)+B_7B_{13}\left(B_3B_{15}-B_5B_{14}\right)$$

$$b_5=B_1B_4\left(B_7B_{11}B_{15}+B_9B_{12}B_{14}\right)+B_1B_8B_{12}\left(B_3B_{15}-B_5B_{14}\right)+B_1B_4B_6B_{12}B_{15}+B_1B_7B_{13}\left(B_5B_{14}+B_3B_{15}\right)$$
$$+B_2B_{10}\left(B_5B_7B_{11}+B_3B_9B_{12}+B_5B_6B_{12}-B_5B_7B_{14}+B_3B_7B_{15}\right)$$

We again adopted Routh- Hurwitz criterion for stability to investigate the stability of (7.6)
For order five;

$$b_0\lambda^5+b_1\lambda^4+b_2\lambda^3+b_3\lambda^2+b_4\lambda+b_5=0$$

But $b_0=1$ in (7.6). Thus,

$$\Delta_5=\begin{vmatrix} b_1 & b_3 & b_5 & 0 & 0 \\ 1 & b_2 & b_4 & 0 & 0 \\ 0 & b_1 & b_3 & b_5 & 0 \\ 0 & 1 & b_2 & b_4 & 0 \\ 0 & 0 & b_1 & b_3 & b_5 \end{vmatrix}$$

This gives,

$$\Delta_1 = b_1, \Delta_2 = \begin{vmatrix} b_1 & b_3 \\ 1 & b_2 \end{vmatrix}, \Delta_3 = \begin{vmatrix} b_1 & b_3 & b_5 \\ 1 & b_2 & b_4 \\ 0 & b_1 & b_3 \end{vmatrix} \Rightarrow \Delta_3 = b_1 b_2 b_3 - b_1^2 b_4 - b_3^2 + b_1 b_5,$$

$$\Delta_4 = \begin{vmatrix} b_1 & b_3 & b_5 & 0 \\ 1 & b_2 & b_4 & 0 \\ 0 & b_1 & b_3 & b_5 \\ 0 & 1 & b_2 & b_4 \end{vmatrix} \Rightarrow b_5 \begin{vmatrix} b_1 & b_3 & b_5 \\ 1 & b_2 & b_4 \\ 0 & 1 & b_2 \end{vmatrix} - b_4 \begin{vmatrix} b_1 & b_3 & b_5 \\ 1 & b_2 & b_4 \\ 0 & b_1 & b_3 \end{vmatrix}$$

$$\Delta_4 = b_5 \left[b_1 \left(b_2^2 - b_4 \right) - b_3 \left(b_2 \right) + b_5 \right] - b_4 \left[b_1 \left(b_2 b_3 - b_1 b_4 \right) - b_3^2 + b_1 b_5 \right]$$

$$\Delta_4 = b_1 b_2^2 b_5 - b_1 b_4 b_5 - b_2 b_3 b_5 + b_5^2 - b_1 b_2 b_3 b_4 + b_1^2 b_4^2 + b_3^2 b_4 - b_1 b_4 b_5$$

Thus,

$$\Delta_5 = b_5 \Delta_4 = b_5 \left(b_1 b_2^2 b_5 - 2 b_1 b_4 b_5 - b_2 b_3 b_5 + b_5^2 - b_1 b_2 b_3 b_4 + b_1^2 b_4^2 + b_3^2 b_4 \right)$$

$$\Delta_5 = b_1 b_2^2 b_5^2 - 2 b_1 b_4 b_5^2 - b_2 b_3 b_5^2 + b_5^3 - b_1 b_2 b_3 b_4 b_5 + b_1^2 b_4^2 b_5 + b_3^2 b_4 b_5 > 0$$

Thus, by Routh Hurwitz criteria, the determinant of equation (7.6) is given by

$$b_1 b_2^2 b_5^2 - 2 b_1 b_4 b_5^2 - b_2 b_3 b_5^2 + b_5^3 - b_1 b_2 b_3 b_4 b_5 + b_1^2 b_4^2 b_5 + b_3^2 b_4 b_5 > 0$$

. The roots $\lambda_1, \lambda_2, \lambda_3, \lambda_4,$ and λ_5 will have negative real parts provided that;

$$b_1 b_2^2 b_5^2 + b_5^3 + b_1^2 b_4^2 b_5 + b_3^2 b_4 b_5 > 2 b_1 b_4 b_5^2 + b_2 b_3 b_5^2 + b_1 b_2 b_3 b_4 b_5$$

(Routh Hurwitz criteria) holds. Therefore, the equilibrium points at temperature $T = 0$, $E_1 = \left(N^*, Z^*, O^*, P^*, 0, G^* \right)$ is locally asymptotically stable.

IX. NUMERICAL SIMULATION

In this section, numerical simulations are conducted to validate the applicability of the theoretical findings. To achieve this, the following parameter values are selected for the model system (3.0) -(3.5).

Table 3: Parameter values used in numerical simulation

Parameter	Description	Values	Literature Source
D	Washout rate	$0.4 \left(1 day^{-1} \right)$	Macdonald & Gulbudak (2023)
w	Microbial decomposition efficiency factor	0.4	Roy Chowdhury et al. (2023)
N_0	Constant input of nutrient concentration	$40 \left(mgdm^{-3} \right)$	Rehim *et al.* (2016)
a	Half-saturation constant	$1.0 \left(mgdm^{-3} \right)$	Rehim *et al.* (2016)
x	Temperature decrease rate	$0.1 \left(day^{-1} \right)$	Assumed
v	Self-shading	$0.02 \left(\left(mgdm^{-3} \right)^{-1} day^{-1} \right)$	Assumed
k_1	Conversion factor from nutrient to phytoplankton	0.5	Macdonald & Gulbudak (2023)
k_2	Conversion factor from phytoplankton to zooplankton	0.4	Assumed
k_3	Toxic substance production rate	$0.2 \left(day^{-1} \right)$	Rehim *et al.* (2016)
f	Greenhouse gas increase rate	$0.05 \left(day^{-1} \right)$	Assumed

m_1	Nutrient production from phytoplankton mortality	0.3	Assumed
m_2	Nutrient production from zooplankton mortality	0.25	Assumed
d_1	Natural mortality rate of phytoplankton	$0.1\left(day^{-1}\right)$	Rehim *et al.* (2016)
d_2	Natural mortality rate of zooplankton	$0.08\left(day^{-1}\right)$	Rehim *et al.* (2016)
h	Temperature inhibition rate	$0.03\ \left(day^{-1}\right)$	Roy et al. (2012)
ε	Temperature production rate	$0.01\ \left(day^{-1}\right)$	Assumed
α	Nutrient uptake rate	$0.4\left(1day^{-1}\right)$	Rehim *et al.* (2016)
ϕ	Greenhouse production rate	$0.012\ \left(day^{-1}\right)$	Assumed
β	Maximum zooplankton ingestion rate	$0.6\left(1day^{-1}\right)$	Rehim *et al.* (2016)
δ	Oxygen consumption by decomposition	$0.03\ \left(day^{-1}\right)$	Roy Chowdhury et al. (2023)
ψ	Oxygen production by photosynthesis	$0.5\ \left(day^{-1}\right)$	Assumed
μ	Oxygen depletion due to temperature	$0.02\ \left(day^{-1}\right)$	Assumed
π_1	Oxygen consumption by phytoplankton respiration	$0.01\left(\left(mgdm^{-3}\right)^{-1}day^{-1}\right)$	Assumed
π_2	Oxygen consumption by zooplankton respiration	$0.015\left(\left(mgdm^{-3}\right)^{-1}day^{-1}\right)$	Assumed
π_3	Oxygen depletion due to greenhouse gases	$0.01\left(day^{-1}\right)$	Assumed
σ	Nutrient depletion due to temperature	$0.04\ \left(day^{-1}\right)$	Assumed
θ_1	Temperature increase due to greenhouse gases	$0.025\ \left(day^{-1}\right)$	Assumed
θ_2	Greenhouse gas removal rate	$0.2\ \left(day^{-1}\right)$	Assumed
τ_1	Delay in phytoplankton decomposition	2.5 (days)	Assumed
τ_2	Delay in zooplankton decomposition	4.0 (days)	Assumed
τ_3	Delay for toxic-phytoplankton maturity	5.5 (days)	Assumed

We made use of Matlab dde23 solver to carryout the numerical simulation for the model with delay. And we use Matlab ode45 solver to carryout the numerical simulation for the model without delay i.e at $\tau_1 = \tau_2 = \tau_3 = 0$.

9.1 Simulation Graphs with Delay

© JUL 2026 | IRE Journals | Volume 10 Issue 1 | ISSN: 2456-8880
DOI: https://doi.org/10.64388/IREV10I1-1719581

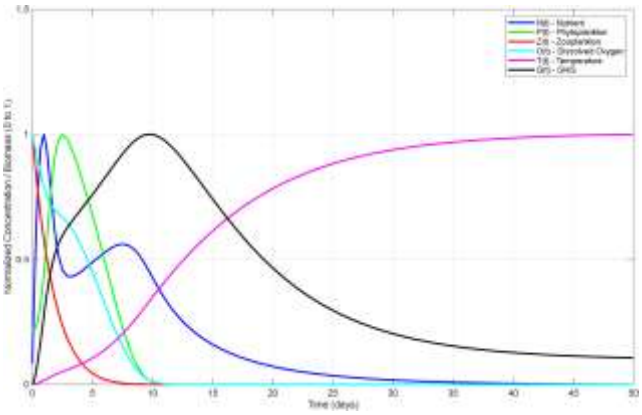

Figure 2: The model simulation

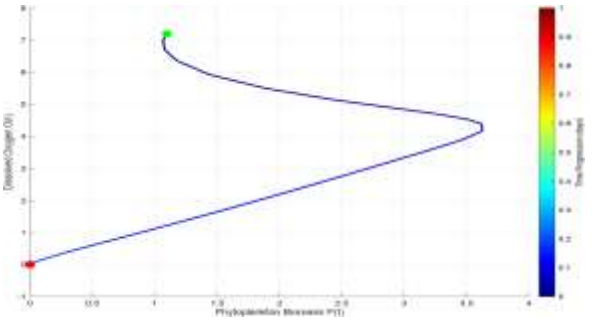

Figure 3: The phase-plane analysis

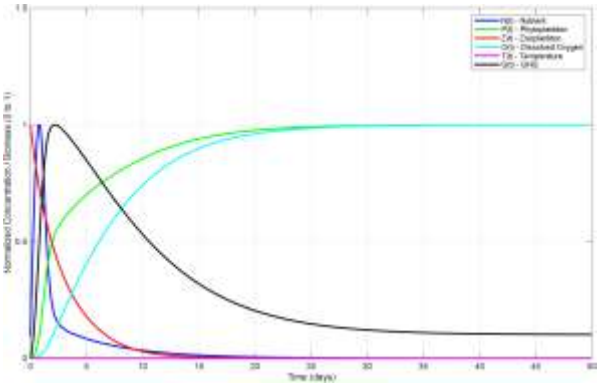

Figure 4: The model simulation for temperature of the upper ocean T=0

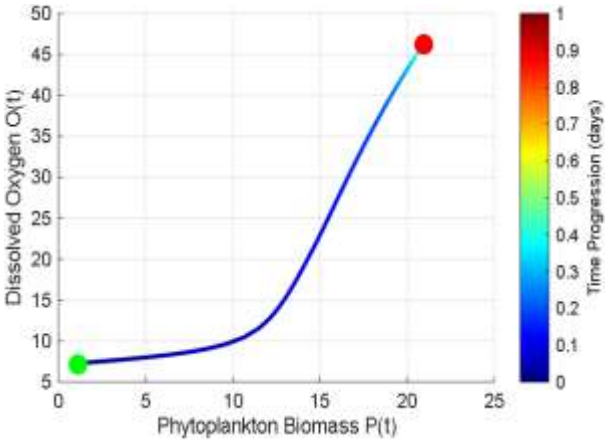

Figure 5: Temperature of the upper ocean, T=0 phase plane

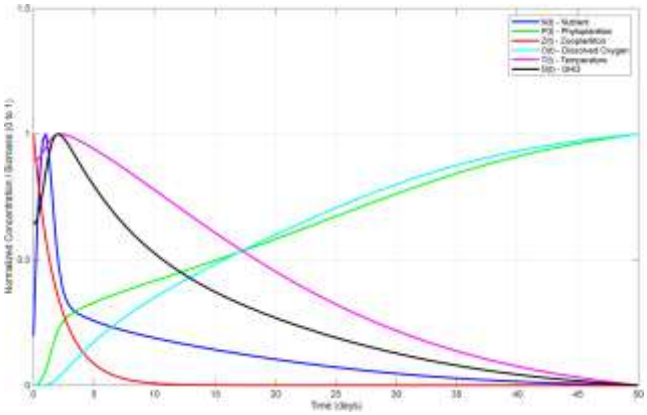

Figure 6: Minimal deoxygenation

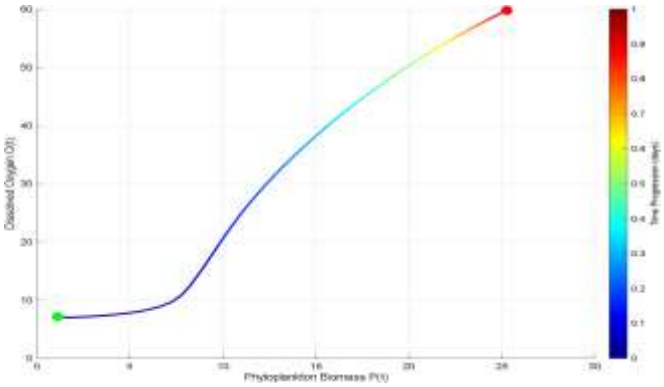

Figure 7: Minimal Phase plane

© JUL 2026 | IRE Journals | Volume 10 Issue 1 | ISSN: 2456-8880
DOI: https://doi.org/10.64388/IREV10I1-1719581

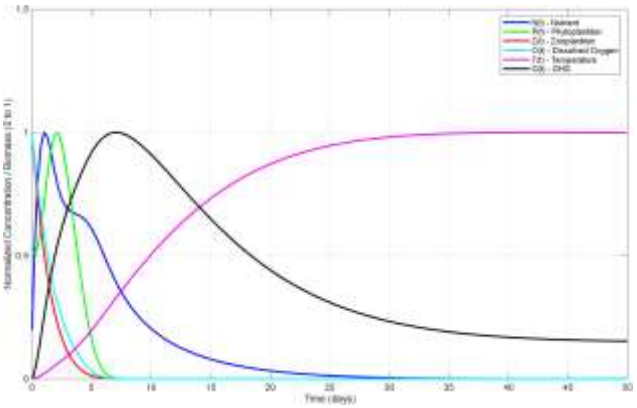

Figure 8: Moderate deoxygenation

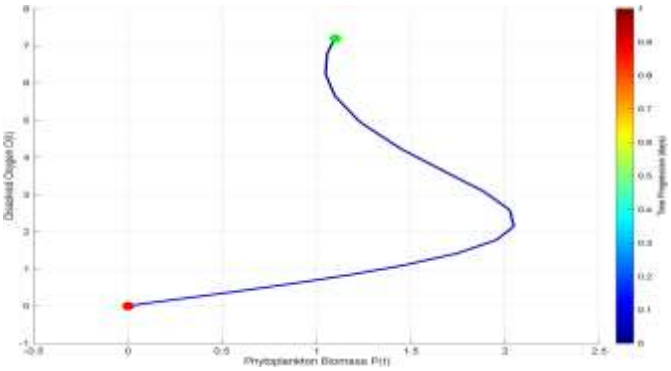

Figure 9: Moderate Phase plane

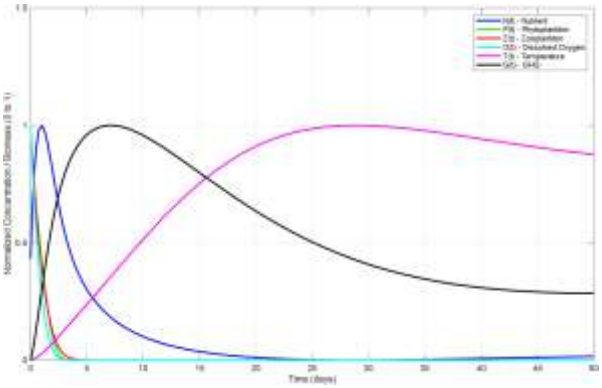

Figure 10: Severe deoxygenation

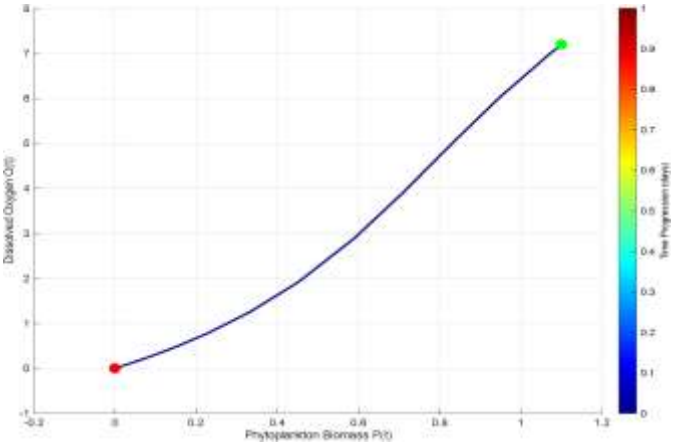

Figure 11: Severe Phase plane

Discussion of the simulation results

Figure 2

The coexistence equilibrium point reveals rapid deoxygenation dynamics in response to interacting biological and physical processes. Dissolved oxygen O(t) declines continuously and sharply, approaching near-anoxic conditions by day 15.

This persistent oxygen loss occurs despite an early phytoplankton bloom (peaking around day 3–4), indicating the distinct behavior of deoxygenation in a system where oxygen production is the primary function of phytoplankton. The subsequent collapse of phytoplankton biomass further limits oxygen replenishment, creating positive feedback that accelerates hypoxia development.

These results demonstrate how climate-driven warming and greenhouse gas forcing can trigger rapid and sustained deoxygenation, even following transient phytoplankton blooms, highlighting the critical sensitivity of marine oxygen budgets to interactive biophysical feedbacks.

Figure 3

The phase-plane analysis between phytoplankton biomass P(t) and dissolved oxygen O(t) reveals a pronounced hysteresis-like behavior and strong deoxygenation feedback in the model. The system begins near the origin, with both phytoplankton and oxygen concentrations starting at very low levels (P≈0 and O≈0). In the early phase, phytoplankton

biomass increases rapidly, triggering a sharp rise in dissolved oxygen O(t).

However, as phytoplankton biomass continues to grow beyond this point, the relationship reverses at high phytoplankton biomass, where P(t)≈3.75 and O(t)≈4.3. Oxygen levels begin to decline steadily even as phytoplankton density keeps increasing. This shift marks the transition from net oxygen production to net oxygen consumption.

Oxygen levels begin to increase again and peaks at approximately 7.2 units when phytoplankton biomass P(t) is approximately 1.1. Several interconnected processes drive this deoxygenation, including elevated community respiration, temperature-induced oxygen loss, microbial decomposition of organic matter, and reduced photosynthetic efficiency caused by self-shading and toxic substances released by dense phytoplankton populations.

The resulting counter-clockwise trajectory is particularly revealing: for the same level of phytoplankton biomass, oxygen concentrations are noticeably higher during the growth phase than during the later bloom phase.

This dynamic closely mirrors real-world observations of hypoxia development following intense phytoplankton blooms in coastal and marine ecosystems. This suggests the possible emergence of a quasi-stable degraded state marked by persistent deoxygenation.

Figure 4
the deoxygenation scenario for the equilibrium points at T(t)=0 demonstrates a relatively stable and resilient marine ecosystem. Initially, nutrient availability promotes rapid phytoplankton growth P(t), which subsequently enhances dissolved oxygen concentration O(t) through photosynthetic activity. This behavior is supported by the comparatively high oxygen production rate (ψ = 0.50) and the low decomposition oxygen demand (δ = 0.03).

Since temperature is fixed at zero, warming-induced oxygen depletion (μTO = 0) and thermal inhibition of phytoplankton growth (hTP = 0) are completely eliminated, allowing oxygen levels to increase steadily and stabilize near their maximum values.

Although zooplankton biomass Z(t) gradually declines over time, greenhouse gas concentration decreases after an initial increase because greenhouse gas removal remains moderately effective (θ_2 = 0.20).

Overall, the results suggest that at T(t)=0 temperature effects significantly improve oxygen stability, enhances phytoplankton persistence, and increases ecosystem resilience against deoxygenation stress.

Figure 5
The phase plane for the temperature T=0 deoxygenation scenario shows a healthier and more stable relationship between phytoplankton biomass P(t) and dissolved oxygen O(t). As phytoplankton biomass increases, oxygen concentration also rises steadily, indicating that photosynthesis is effectively supplying oxygen to the system.

This behavior is supported by the relatively high oxygen production rate (ψ = 0.50), together with low oxygen loss from decomposition (δ = 0.03) and weak warming-related oxygen depletion (μ = 0.02).

In addition, the mild temperature stress on phytoplankton (h = 0.03) allows phytoplankton to persist and continue producing oxygen efficiently.

Unlike the moderate and severe scenarios, the trajectory moves smoothly toward a high-oxygen state, suggesting improved ecosystem stability, stronger biological productivity, and greater resilience against deoxygenation stress.

Figure 6
We adjusted some of the parameter's values in order to test minimal deoxygenating. Parameter values used in this simulation correspond to the minimal deoxygenation case, notably strong photosynthetic oxygen production (ψ=0.65), low oxygen consumption rates (δ=0.02, μ=0.008, π_1=0.01, π_2

=0.012, π_3=0.005), weak temperature inhibition (h=0.015), and efficient greenhouse gas removal (θ_2=0.25).

We also considered high nutrient uptake efficiency (α=0.48, k_1=0.5), low self-shading effect (v=0.015), and minimal temperature inhibition on growth (h=0.015).

The simulation reveals highly favorable oxygen dynamics. Dissolved oxygen O(t) exhibits a strong and consistent increasing trend throughout the 50-day period, eventually approaching its maximum normalized value.

This sustained oxygenation is primarily driven by the high photosynthetic oxygen production rate (ψ=0.65), which significantly outweighs oxygen-consuming processes. Phytoplankton biomass P(t) shows robust growth after an initial lag, becoming the dominant biological compartment by the end of the simulation.

A striking feature is the rapid collapse of zooplankton biomass Z(t) within the first 5–7 days, after which it remains near zero. The relatively low zooplankton conversion efficiency (k_2=0.4) and moderate ingestion rate (β=0.6) limit top-down control, allowing phytoplankton to grow with minimal grazing pressure. This trophic imbalance further enhances net oxygen production.

Nutrient concentration N(t) is rapidly depleted after a brief initial peak, indicating efficient biological uptake by the expanding phytoplankton population. Both temperature T(t) and greenhouse gas concentration G(t) show declining trends, consistent with the low GHG production (ϕ=0.01), slow warming rate (θ_1=0.012), and strong removal rate (θ_2=0.25).

The resulting lower temperature helps maintain higher oxygen solubility and reduces metabolic oxygen demand.

Figure 7
The phase plane for the minimal deoxygenation scenario shows a strong positive relationship between phytoplankton biomass P(t) and dissolved oxygen O(t). As phytoplankton increases, oxygen concentration also rises steadily due to efficient photosynthetic oxygen production (ψ = 0.65).

The smooth upward trajectory indicates a stable ecosystem where oxygen production exceeds oxygen loss.

Figure 8
The moderate deoxygenation scenario captured shows the marine ecosystem experiencing significant environmental stress. At the beginning of the simulation, the relatively high nutrient input (N_0 = 40) supports a rapid increase in phytoplankton biomass, leading to a bloom within the first few days.

However, this bloom quickly collapses as nutrients are depleted and temperature-induced inhibition (h = 0.04) begins to suppress phytoplankton growth.

Zooplankton biomass declines steadily throughout the simulation. Although food is initially available, the combined effects of warming, oxygen depletion, and environmental stress prevent the zooplankton population from sustaining long-term growth.

One of the most noticeable features of the plot is the rapid decline in dissolved oxygen concentration. Oxygen levels fall sharply toward near-zero values because oxygen consumption from decomposition (δ = 0.05), warming-driven oxygen loss (μ= 0.035), and biological respiration exceeds oxygen production.

In this scenario, the phytoplankton oxygen production rate is only moderate (ψ = 0.45), making it insufficient to compensate for the increasing oxygen demand.

At the same time, temperature rises continuously due to greenhouse gas forcing. This warming is influenced by the greenhouse-gas-to-temperature conversion rate (θ_1 = 0.035) and the moderate greenhouse gas removal rate (θ_2 = 0.15).

Greenhouse gas concentration initially increases, reaches a peak, and later declines gradually as natural removal processes become effective. Nevertheless, the temporary greenhouse gas accumulation is enough to maintain elevated temperatures and intensify oxygen depletion.

Figure 9
The phase plane for the moderate deoxygenating scenario shows that both phytoplankton biomass P(t) and dissolved oxygen O(t) rise at the beginning because nutrients are still available (N_0 = 40) and phytoplankton can still produce oxygen at a moderate rate (ψ = 0.45).

However, this improvement is only temporary. As time progresses, oxygen levels begin to fall due to increased oxygen consumption from decomposition (δ = 0.05), warming-related oxygen loss (μ = 0.035), and temperature stress on phytoplankton (h = 0.04).

Eventually, both oxygen concentration and phytoplankton biomass decline, showing that the ecosystem is becoming unstable. Unlike the minimal deoxygenation case, the system cannot sustain high oxygen levels, indicating growing hypoxia and weakening marine productivity.

Figure 10
The severe deoxygenating scenario shows a highly stressed and unstable marine ecosystem driven by stronger warming effects and rapid oxygen depletion.

In this case, the ecosystem is influenced by low oxygen production (ψ = 0.28), high decomposition oxygen demand (δ = 0.12), strong warming-induced oxygen loss (μ = 0.07), and severe phytoplankton inhibition due to temperature ((h = 0.08).

At the beginning of the simulation, nutrient concentration N(t) increases briefly because of the high nutrient input (N_0 = 50). However, nutrients are rapidly consumed and later decline toward very low levels as biological activity and environmental stress intensify.

Unlike the moderate scenario, phytoplankton P(t) and zooplankton Z(t) collapse almost immediately. Although nutrients are abundant initially, the strong temperature stress, high toxicity (k_3 = 0.25), and rapid oxygen depletion prevent plankton populations from sustaining growth.

The phytoplankton bloom is extremely short-lived, while zooplankton quickly approaches extinction due to lack of oxygen and food availability.

Dissolved oxygen O(t) decreases very rapidly and reaches near-zero values within a short time. This sharp decline occurs because oxygen consumption from decomposition and warming greatly exceeds oxygen generation. The low oxygen production rate (ψ = 0.28) is unable to compensate for the strong oxygen losses caused by decomposition (δ = 0.12), respiration, and greenhouse-gas-related effects.

Temperature (T(t)) rises steadily and remains very high throughout the simulation due to strong greenhouse forcing (θ_1 = 0.06) and weak greenhouse gas removal (θ_2 = 0.08).

Although greenhouse gas concentration (G(t)) later declines gradually, its initial accumulation is large enough to maintain long-term warming and ecological stress.

Overall, the severe deoxygenation scenario predicts rapid ecosystem degradation characterized by oxygen collapse, loss of plankton populations, persistent warming, and reduced biological stability.

Compared with the moderate scenario, the severe case exhibits much faster oxygen depletion, stronger warming effects, and near-total collapse of marine biological activity.

The phase plane for the severe deoxygenation scenario (Figure 11) shows that the marine ecosystem is under extreme environmental stress.

Both phytoplankton biomass P(t) and dissolved oxygen O(t) remain very low throughout the simulation, indicating weak biological activity and poor oxygen conditions. Unlike the minimal and

© JUL 2026 | IRE Journals | Volume 10 Issue 1 | ISSN: 2456-8880
DOI: https://doi.org/10.64388/IREV10I1-1719581

moderate scenarios, the system is unable to sustain healthy oxygen levels or plankton productivity, suggesting a highly unstable ecosystem with persistent hypoxia and reduced ecological resilience.

9.2 Simulation Graphs without Delay ($\tau_1 = \tau_2 = \tau_3 = 0$)

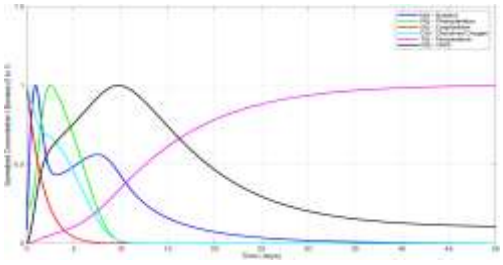

Figure 12: The model simulation

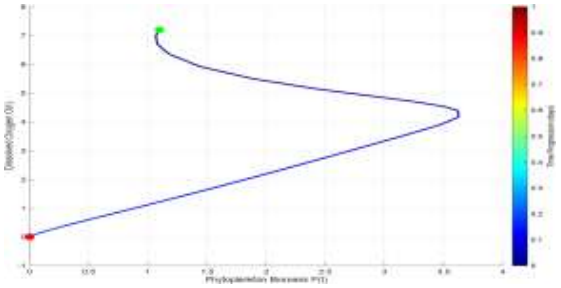

Figure 13: Phase plane

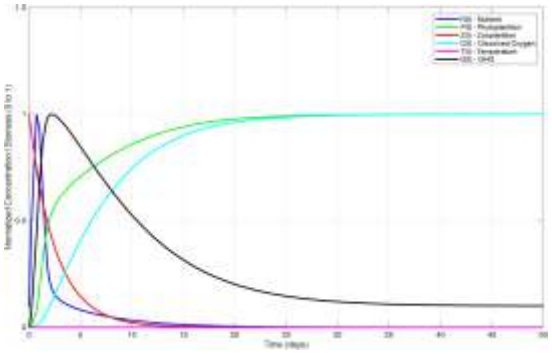

Figure 14: The model simulation for temperature of the upper ocean T=0

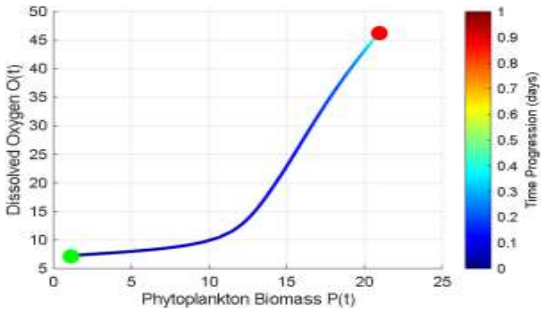

Figure 15: Temperature of the upper ocean, T=0 phase plane

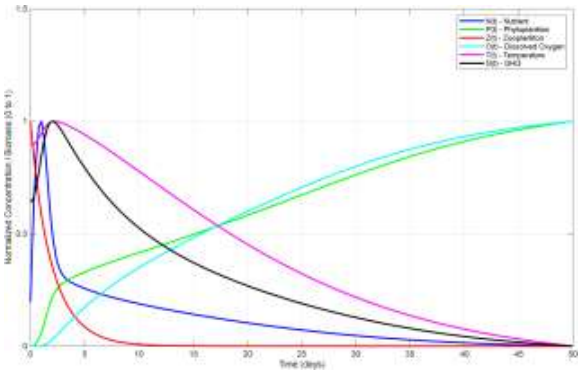

Figure 16: Minimal deoxygenation

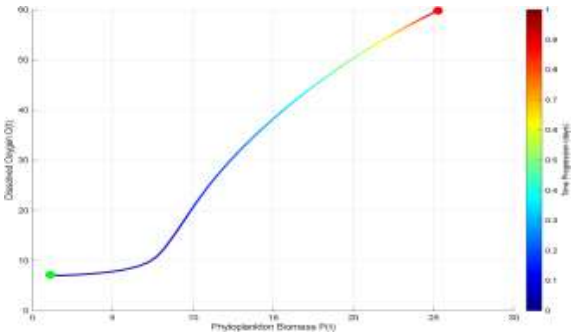

Figure 17: Minimal Phase plane

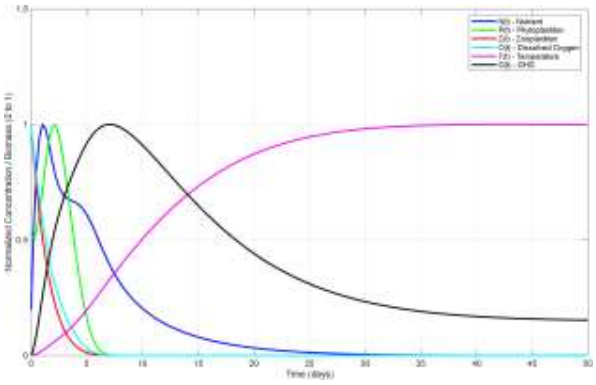

Figure 18: Moderate deoxygenation

© JUL 2026 | IRE Journals | Volume 10 Issue 1 | ISSN: 2456-8880
DOI: https://doi.org/10.64388/IREV10I1-1719581

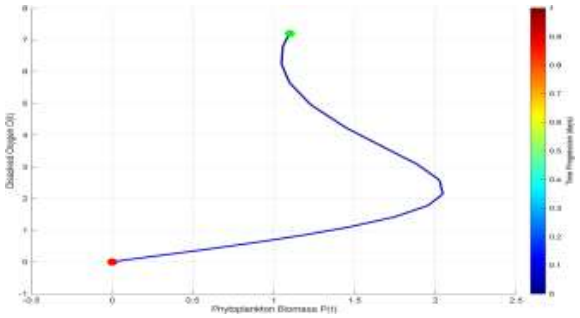

Figure 19: Moderate Phase plane

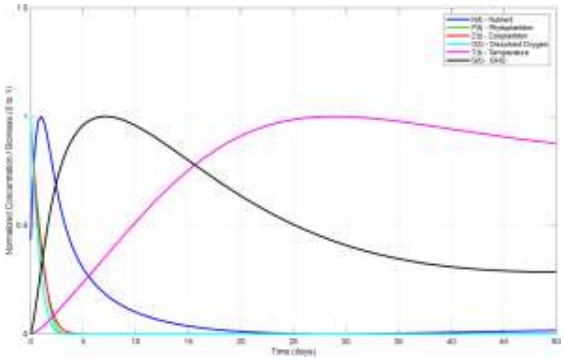

Figure 20: Severe deoxygenation

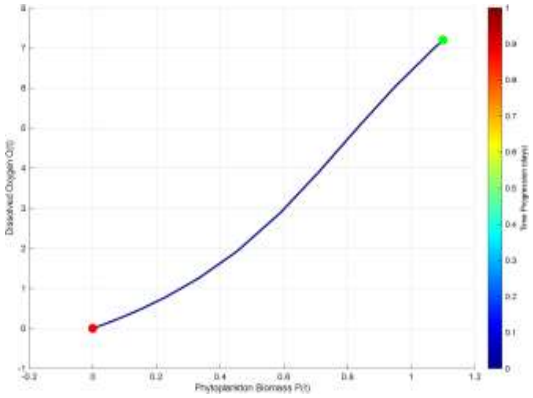

Figure 21: Severe Phase plane

Using the parameter values in Table 3, the numerical simulations obtained with the MATLAB ode45 solver (without delay) are identical to those obtained with the dde23 solver (with delays (τ_1=2.5, τ_2 =4.0, and τ_3=5.5 days). The temporal dynamics of all state variables in Figures 2 and 12 show the same qualitative behavior, while the corresponding phase-plane trajectories of dissolved oxygen (O(t)) versus phytoplankton biomass (P(t)) in Figures 3 and 13 also coincide.

Similarly, identical responses are observed under the minimal deoxygenation scenario (Figures 6 and 16) and their corresponding phase planes (Figures 7 and 17), the moderate deoxygenation scenario (Figures 8 and 18) and their phase planes (Figures 9 and 19), as well as the severe deoxygenation scenario (Figures 10 and 20) and their corresponding phase planes (Figures 11 and 21).

These results demonstrate that the incorporation of the selected biological delays does not alter the qualitative dynamics of the system, indicating that the delays are below the critical threshold required to influence long-term ecosystem behavior. Thus, the delays affect only the transient response, while the equilibrium dynamics remain unchanged.

Conclusions and recommendation

The delayed and non-delayed models produce identical dynamics because the imposed delays (τ_1=2.5, τ_2 =4.0, and τ_3=5.5 days) are below the critical threshold required to alter the system's stability. Hence, the delays affect only the transient response and not the equilibrium behavior.

Biologically, this indicates that short-term delays in plankton decomposition, and toxin maturation have minimal influence on ecosystem dynamics under favorable environmental conditions. Environmentally, the results suggest that ocean deoxygenation is governed primarily by climate-related factors, such as warming, greenhouse gas accumulation, and nutrient loading, rather than by short biological time lags.

As an extension of this work, a systematic delay-induced bifurcation analysis is recommended to examine the influence of time delays on the stability, periodicity, and overall dynamics of the proposed model.

REFERENCES

[1] Akagha, S. C., Nwankwo, D. I., & Yin, K. (2020). Dynamics of nutrient and phytoplankton in Epe Lagoon, Nigeria: possible causes and consequences of reoccurring cyanobacterial blooms. Applied Water Science, 10(5), 109.

[2] Carpenter, S. R., Caraco, N. F., Correll, D. L., Howarth, R. W., Sharpley, A. N., & Smith, V. H. (1998). Nonpoint pollution of surface waters with phosphorus and nitrogen. Ecological applications, 8(3), 559–568.

[3] Chen, M., Fan, M., Liu, R., Wang, X., Yuan, X., & Zhu, H. (2015). The dynamics of temperature and light on the growth of phytoplankton. Journal of Theoretical Biology, 385, 8–19.

[4] Cheng, L., Abraham, J., Trenberth, K. E., Boyer, T., Mann, M. E., & Zhu, J. (2024). New record ocean temperatures and related climate indicators in 2023. Advances in Atmospheric Sciences, 41(6), 1068–1082.

[5] Cheng, L., Pan, Y., Tan, Z., Zheng, H., Zhu, Y., & Wei, W. (2024). IAPv4 ocean temperature and ocean heat content gridded dataset. Earth System Science Data, 16(8), 3517–3546.

[6] Chowdhury, P. R., Banerjee, M., & Petrovskii, S. (2024). A two-timescale model of plankton–oxygen dynamics predicts formation of oxygen minimum zones and global anoxia. Journal of Mathematical Biology, 89(1), 8.

[7] Crain, C. M., Kroeker, K., & Halpern, B. S. (2008). Interactive and cumulative effects of multiple human stressors in marine systems. Ecology Letters, 11(12), 1304–1315.

[8] Devlin, M., & Brodie, J. (2023). Nutrients and eutrophication. In Marine pollution–monitoring, management and mitigation (pp. 75–100). Springer.

[9] Dybas, C. L. (2005). Dead zones spreading in world oceans. BioScience, 55(7), 552–557.

[10] Gulev, S. K., Thorne, P. W., Ahn, J., Dentener, F. J., Domingues, C. M., & Gerland, S. (2021). Changing state of the climate system.

[11] Halpern, B. S.,Walbridge, S., Selkoe, K. A., Kappel, C. V., Micheli, F., & d'Agrosa, C. (2008). A global map of human impact on marine ecosystems. Science, 319(5865), 948–952.

[12] Hartmann, D. L., Tank, A. M. K., Rusticucci, M., Alexander, L. V., Br¨onnimann, S., Charabi, Y. A. R., *et al.* (2013). Observations: atmosphere and surface. In Climate change 2013 the physical science basis: Working group i contribution to the fifth assessment report of the intergovernmental panel on climate change (pp. 159–254). Cambridge University Press.

[13] Houghton, J. T. (1990). Climate change: the IPCC scientific assessment; report prepared for IPCC by working group 1. Cambridge University Press.

[14] Johnson, G., & Wijffels, S. (n.d.). Coauthors, 2018: Ocean heat content [in state of the climate in 2017]. Bull. Amer. Meteor. Soc, 99(8), S72–S77.

[15] Kolodziejczyk, N., Portela, E., Thierry, V., & Prigent, A. (2024). ISASO2: Recent trends and regional patterns of ocean dissolved oxygen change. Earth System Science Data, 16(11), 5191–5206.

[16] Laffoley, D., & Baxter, J. M. (2019). Ocean deoxygenation: Everyone's problem: causes, impacts, consequences and solutions. IUCN Gland, Switzerland.

[17] Le Qu´er´e, C., Takahashi, T., Buitenhuis, E. T., R¨odenbeck, C., & Sutherland, S. C. (2010). Impact of climate change and variability on the global oceanic sink of CO2. Global Biogeochemical Cycles, 24(4).

[18] Li, T., Li, X., Zheng, Y., Zhu, P., Zhang, C., Zhang, K., & Xu, J.-J. (2023). Phosphorescent carbon dots as long-lived donors to develop an energy transfer-based sensing platform. Analytical Chemistry, 95(4), 2445–2451.

[19] Loeb, N. G., Johnson, G. C., Thorsen, T. J., Lyman, J. M., Rose, F. G., & Kato, S. (2021). Satellite and ocean data reveal marked increase in Earth's heating rate. Geophysical Research Letters, 48(13), e2021GL093047.

[20] Macdonald, J. C., & Gulbudak, H. (2023). Forward hysteresis and hopf bifurcation in an npzd model with application to harmful algal blooms. arXiv preprint arXiv:2307.06234.

[21] Mandal, S., Islam, M. S., & Biswas, M. H. A. (2021a). Modeling the potential impact of

climate change on living beings near coastal areas. Modeling Earth Systems and Environment, 7, 1783–1796.

[22] Mandal, S., Islam, M. S., & Biswas, M. H. A. (2021b). Modeling and analytical analysis of the effect of atmospheric temperature to the planktonic ecosystem in oceans. In Applications of internet of things: Proceedings of icccciot 2020 (pp. 131–140).

[23] Martin, D., McKenna, H., & Livina, V. (2017). The human physiological impact of global deoxygenation. The journal of physiological sciences, 67, 97–106.

[24] Mikaloff Fletcher, S. E., Gruber, N., Jacobson, A. R., Doney, S. C., Dutkiewicz, S., Gerber, M., *et al.* (2006). Inverse estimates of anthropogenic CO2 uptake, transport, and storage by the ocean. Global biogeochemical cycles, 20(2).

[25] Nixon, S. W. (1998). Enriching the sea to death. Scientific American, 9(3), 48–53.

[26] NOAA. (2024, June 16). Ocean oxygen. https://oceanservice.noaa.gov/facts/ ocean-oxygen.html. (National Oceanic and Atmospheric Administration)

[27] NOAA. (2025, February 9). Trends in CO2-noaa global monitoring laboratory. https:// www.esrl.noaa.gov/gmd/ccgg/trends/. (National Oceanic and Atmospheric Administration)

[28] Ochieng, F. O. (2024). A novel data-driven dynamical model for predicting future climate trends. Modeling Earth Systems and Environment, 10(4), 4599–4610.

[29] Octavina, C., Maghfirah, M., Lacroix, G., Suciati, N., Fajar, M., Syufi, N. H., Haditiar, Y., *et al.* (2025). Spatial analysis of plankton distribution in northern waters of aceh: An indicator of marine environmental quality. In BIO Web of conferences (Vol. 156, p. 02005).

[30] Olson, S., Jansen, M. F., Abbot, D. S., Halevy, I., & Goldblatt, C. (2022). The effect of ocean salinity on climate and its implications for Earth's habitability. Geophysical research letters, 49(10), e2021GL095748.

[31] Pachauri, R., Meyer, L., Team, C. W., et al. (2014). Ipcc: Geneva. Switzerland.

[32] Pachiappan, P., Santhanam, P., Begum, A., & Balaji Prasath, B. (2019). An introduction to plankton. Basic and applied phytoplankton biology, 1–24.

[33] Prentice, I. C., Farquhar, G., Fasham, M., Goulden, M. L., Heimann, M., Jaramillo, V., *et al.* (2001). The carbon cycle and atmospheric carbon dioxide. Climate change 2001: the scientific basis, Intergovernmental panel on climate change.

[34] Rehim, M., Zhang, Z., & Muhammadhaji, A. (2016). Mathematical analysis of a nutrient–plankton system with delay. SpringerPlus, 5, 1–22.

[35] Rhein, M., Rintoul, S. R., Aoki, S., Campos, E., Chambers, D., Feely, R. A., *et al.* (2013). Observations: ocean.

[36] Roy, S., Broomhead, D. S., Platt, T., Sathyendranath, S., & Ciavatta, S. (2012). Sequential variations of phytoplankton growth and mortality in an npz model: A remote-sensingbased assessment. Journal of Marine Systems, 92(1), 16–29.

[37] Sabine, C. L., Feely, R. A., Gruber, N., Key, R. M., Lee, K., Bullister, J. L., *et al.* (2004). The oceanic sink for anthropogenic CO2. Science, 305(5682), 367–371.

[38] Sarkar, K., Nieto, J. J., Khajanchi, S., & Mali, P. C. (2025). Modeling the influence of global warming on carbon, phytoplankton, and zooplankton dynamics. Scientific Reports, 15(1), 17911.

[39] Scavia, D., Ludsin, S. A., Michalak, A. M., Obenour, D. R., Han, M., Johnson, L. T., Zhou, Y., *et al.* (2024). Water quality–fisheries tradeoffs in a changing climate underscore the need for adaptive ecosystem–based management. Proceedings of the National Academy of Sciences, 121(45), e2322595121.

[40] Schmidtko, S., Stramma, L., & Visbeck, M. (2017). Decline in global oceanic oxygen

content during the past five decades. Nature, 542(7641), 335–339.

[41] Sekerci, Y., & Ozarslan, R. (2020). Respiration effect on plankton–oxygen dynamics in view of non-singular time fractional derivatives. Physica A: Statistical Mechanics and its Applications, 553, 123942.

[42] Sekerci, Y., & Petrovskii, S. (2015). Mathematical modelling of plankton–oxygen dynamics under the climate change. Bulletin of Mathematical Biology, 77, 2325–2353.

[43] Smith, V. H., & Schindler, D. W. (2009). Eutrophication science: where do we go from here? Trends in ecology & evolution, 24(4), 201–207.

[44] Statista. (2024). Atmospheric concentration of CO2 (historic). https://www.statista.com/statistics/1091926/atmospheric-concentration-of-CO2-historic/. (Statista)

[45] Sterpu, M., Rocs, oreanu, C., Efrem, R., & Campbell, S. A. (2023). Stability and bifurcations in a nutrient–phytoplankton–zooplankton model with delayed nutrient recycling with gamma distribution. Mathematics, 11(13), 2911.

[46] Thakur, N. K., Ojha, A., Tiwari, P. K., & Upadhyay, R. K. (2021). An investigation of delay induced stability transition in nutrient-plankton systems. Chaos, Solitons & Fractals, 142, 110474.

[47] Venegas, R. M., Acevedo, J., & Treml, E. A. (2023). Three decades of ocean warming impacts on marine ecosystems: A review and perspective. Deep Sea Research Part II: Topical Studies in Oceanography, 212, 105318.

[48] Von Schuckmann, K., Cheng, L., Palmer, M. D., Tassone, C., Aich, V., Adusumilli, S., *et al.* (2020). Heat stored in the Earth system: Where does the energy go? the gcos Earth heat inventory team. Earth System Science Data Discussions, 2020, 1–45.

[49] Wadanambi, R., Wandana, L., Chathumini, K., Dassanayake, N., Preethika, D., & Arachchige, U. (2020). The effects of industrialization on climate change. J. Res. Technol. Eng, 1(4), 86–94.

[50] Wang, D., Liu, B., Wang, Y., Yang, J., Du, T., Shi, K., *et al.* (2026). Multi-dimensional characterization of seasonal phytoplankton community dynamics in urban water bodies of beijing. Diversity, 18(2), 98.

[51] Yoro, K. O., & Daramola, M. O. (2020). CO2 emission sources, greenhouse gases, and the global warming effect. In Advances in carbon capture (pp. 3–28). Elsevier.

[52] Zhu, J., Kumar, A., Huang, B., Balmaseda, M. A., Hu, Z.-Z., Marx, L., & Kinter III, J. L. (2016). The role of off-equatorial surface temperature anomalies in the 2014 El Niño prediction. Scientific Reports, 6(1), 19677.